

1995

A personal identification biometric system based on back-of-hand vein patterns

A. J. Mehnert
Edith Cowan University

J. M. Cross
Edith Cowan University

C. L. Smith
Edith Cowan University

K. Y. Chia
Edith Cowan University

Follow this and additional works at: <https://ro.ecu.edu.au/ecuworks>



Part of the [Physical Sciences and Mathematics Commons](#)

Mehnert, A. J., Cross, J.M., Smith, C.L., & Chia, K.Y. (1995), *A personal identification biometric system based on back-of-hand vein patterns*. Perth, Australia: Australian Institute of Security and Applied Technology, Edith Cowan University.

This Report is posted at Research Online.
<https://ro.ecu.edu.au/ecuworks/6736>

Edith Cowan University

Copyright Warning

You may print or download ONE copy of this document for the purpose of your own research or study.

The University does not authorize you to copy, communicate or otherwise make available electronically to any other person any copyright material contained on this site.

You are reminded of the following:

- Copyright owners are entitled to take legal action against persons who infringe their copyright.
- A reproduction of material that is protected by copyright may be a copyright infringement.
- A court may impose penalties and award damages in relation to offences and infringements relating to copyright material. Higher penalties may apply, and higher damages may be awarded, for offences and infringements involving the conversion of material into digital or electronic form.

A Personal Identification Biometric System Based on Back-of-Hand Vein Patterns

A.J. MEHNERT, J.M. CROSS, C.L. SMITH, and K.Y. CHIA



Australian Institute of Security and Applied Technology

Edith Cowan University
Perth, Western Australia

{A.Mehnert, J.Cross, Clifton.Smith, K.Chia}@cowan.edu.au

ABSTRACT

This report describes research on the use of back-of-hand vein patterns as a means of uniquely identifying people. In particular it describes a prototype biometric system developed by the Australian Institute of Security and Applied Technology (AISAT). This system comprises an infrared cold source, a monochrome CCD camera, a monochrome frame-grabber, a personal computer, and custom image acquisition, processing, registration, and matching software. The image processing algorithms are based on *Mathematical Morphology*. Registration is performed using rotation and translation with respect to the centroid of the two-dimensional domain of a hand. Vein patterns are stored as *medial axis* representations. Matching involves comparing a given medial axis pattern against a library of patterns using constrained *sequential correlation*. The matching is two-fold: a newly acquired signature is matched against a dilated library signature, and then the library signature is matched against the dilated acquired signature; this is necessary because of the positional noise exhibited by the back-of-hand veins. The results of a cross-matching experiment for a sample of 20 adults and more than 100 hand images is detailed. In addition preliminary estimates of the false acceptance rate (FAR) and false rejection rate (FRR) for the prototype system are given. Fuzzy relaxation on an association graph is discussed as an alternative to sequential correlation for the matching of vein signatures. An example is provided (including a C program) illustrating the matching process for a pair of signatures obtained from the same hand. The example demonstrates the ability of the fuzzy relaxation method to deal with segmentation errors.

Keywords - Biometric, Infrared, Fuzzy relaxation, Mathematical Morphology, Medial axis, Pattern matching, Segmentation, Sequential correlation, Registration

1. INTRODUCTION

Wherever security is required, be it to restrict access to buildings or to computer systems, it is necessary to employ an access control system. Traditional access control systems based on passwords, personal identification numbers (PINs), swipe-cards, keys, and so on, offer limited security. They are open to abuse because such systems identify a token or something known and not the actual person. In the case of a remotely accessed computer for instance, if its password is a dictionary word then security can be breached by trial and error; for example, a user can write a program that attempts to access the remote computer by exhaustively selecting words from an electronic dictionary. In the case of stolen or lost cash/credit cards, it is surprising "to learn that over a quarter of . . . cards which are recovered through the system have their activating PIN written on them" (Parks, 1991, p. 181).

The obvious solution to improving security is to *identify the individual* seeking access. Biometric access control systems do just this by *measuring* physiological or behavioural characteristics, i.e. *biological* traits, of the subject; hence the term biometric. Commercially available systems have exploited fingerprints, keyboard typing rhythm, retinal blood vessel patterns, speech, hand geometry, and the dynamics of signature writing. For example the Fingerscan system, developed in Australia, is an opto-electronic finger scanning device that records "three-dimensional data from the finger such as skin undulations, ridges and valleys, reflections and other living characteristics" (Simpson, 1994, p. 8). Other possibilities for biometric access control include face recognition and gait.

All biometric systems require each authorised user to be enrolled. This involves the user presenting the characterising trait to the system one or more times. A library template or signature is then formed from this sample. This template may be stored in a database or encoded on a smart-card. Subsequently, when the user wishes to gain access, the characteristic trait must be presented to the system which then compares this against a single template in the case of a smart-card, or a multitude of templates. The performance and applicability of biometric systems depends upon many factors including:

- (i) whether or not the client population is closed or open; e.g. a population of factory workers as opposed to the population of potential automatic teller machine users,
- (ii) the false acceptance rate (FAR) and false rejection rate (FRR),
- (iii) user reticence; e.g. objections to fingerprints because of their traditional association with criminality,
- (iv) whether or not the technique is invasive; e.g. retinal scans require the back of the eye to be scanned with a laser,
- (v) ease of use,
- (vi) hygiene, and
- (vii) cleanliness; e.g. a clean hand is needed for palm- and fingerprints.

It is not surprising therefore that "a range of biometric systems is in development or in the market, because no one system meets all needs" (Miller, 1994, p. 22). One such system, first reported by MacGregor and Welford (1991), involves verifying user identity on the basis of the pattern of subcutaneous veins on the back of the hand.

The pattern of veins on the back of the hand is particularly interesting because, although the veins are constrained to run between the bones of the knuckles to connect to the fingers, and are constrained where they run over the wrist bones, in between they seem to conform to no particular pattern. Nevertheless the vein pattern seems to be stable over a period of years. (Hawkes & Clayden, 1993, p. 1).

This technique shows promise as a passive, non-invasive means of personal identification. It must be stressed though that the viability of this concept has yet to be established. Hypothesis testing (statistical inference) is needed to determine the validity of the premise that a person's hand vein pattern is unique. To this end it is necessary to build a research biometric system capable of acquiring, automatically processing, and matching vein pattern images; and for which the FAR and FRR can be established. Cambridge Consultants Ltd., in collaboration with the British Technology Group (BTG), have been researching the hand vein pattern concept (which they have called *Veincheck*) with the aim of developing a commercial system. To date the group appears not to have had too much success – "the performance to be expected from a commercial version of such a system can only be conjectured at this stage" is a quote

from a seminar paper presented by BTG in September, 1993 (Hawkes & Clayden, 1993). This position is further supported by the fact that the group contacted AISAT in 1994 expressing an interest in our research.

In a previous research report (Mehnert, Cross, & Smith, 1993) we detailed a low cost infrared (IR) imaging system and semi-automatic segmentation algorithm for the extraction of a vein signature from a digital infrared image of the back of a person's hand. Since then the AISAT research team have refined the imaging system and segmentation algorithms (now completely automatic) and have additionally implemented and are in the process of evaluating a custom matching algorithm. This report summarises these advancements and offers preliminary matching results and estimates of the FAR and FRR.

2. NEAR INFRARED IMAGING

The infrared spectrum is the range of wavelengths from approximately 700 nm to 14000 nm. The near-red part of the spectrum from 700 to 1350 nm is called the *actinic* range. Radiation in this range "can be reflected, transmitted, or emitted through luminescence*", by objects that are not hot themselves" (Newman, 1976, p. 67); incandescent objects such as tungsten filament light bulbs and the sun produce radiation in this range. Beyond the actinic range up to about 5000 nm is the middle infrared radiation characteristic of hot (non-incandescent) objects ranging from heated flatirons (around 400 °C) to a metal saucepan of boiling water (less than 200 °C). The far end of the spectrum, beyond 5000 nm, represents radiation produced by warm objects such as the human body and sun-warmed ground.

Infrared radiation is invisible to the naked eye. However, for the actinic range (non-hot), film emulsions have been devised that enable this radiation to be photographed. Clinical applications of infrared photography have included the study of skin lesions and blood circulatory patterns. It is the latter application that is of relevance to the development of a back-of-hand vein pattern biometric system. The extent to which the vein structure can be seen on the back of a hand, in visible light, varies from person to person. It is influenced by several factors including: the presence of freckles, moles, scars, and hair; ambient temperature; and recent physical exertion. From a photographic standpoint, actinic IR can penetrate human skin tissue to a depth of about 3 mm. In black-and-white such photographs render the subcutaneous vein system visible as a dark grey network against a light grey background. The *reduced* haemoglobin in venous blood absorbs more infrared than the surrounding skin tissue thus providing contrast. Importantly, "instrument readings and photography show that the skin of all races reflects actinic infrared to about the same degree" (Newman, 1976, p. 112). The keratin in hair absorbs most of the incident infrared radiation and thus appears very dark in a black-and-white infrared photograph. "When sparse dark hair lies very close to the body infrared does reflect off the skin to become partially transmitted through the hair" (Newman, 1976, p. 113). Our experiments show this to be the case for back-of-hand infrared images. Whilst infrared images of the back of the hand show a marked improvement in contrast between skin tissue and veins as compared to what can be seen with the naked eye, the quality and extent of the revealed vein structure is highly variable. Newman (1976, p. 117) has stated that

although it is generally agreed that the veins are more noticeable in the infrared photograph than they are visually, the pictures must not be expected always to show a striking network of veins. Indeed, it is a mistake to be disappointed when the pattern is not boldly delineated. Its distinctness depends on the thickness of the overlaying skin, on the degree of venous engorgement, on the condition of the vein walls and on the nearness of the veins to the surface.

Clearly conventional photography is not suitable for use in a biometric system. Rather, a video camera, frame-grabber, and computer are needed to image, store, and process back-of-hand infrared images. Conventional charge-coupled device (CCD) cameras, though principally designed for use in visible light, are sensitive to near infrared wavelengths up to about 1100 nm. The three most common types of CCD sensors used in these cameras are: C-MOS, INTERLINE TRANSFER, and FRAME TRANSFER. Of these, the INTERLINE TRANSFER "chip is known for its high sensitivity to IR lighting" (Pierce, 1993, p. 2.14). Indeed for the two cameras compared in our previous report (Mehnert,

* Visible-light-excited infrared fluorescence

et al., 1993), it was the camera with the INTERLINE TRANSFER chip that had the greatest sensitivity to IR. Figure 1 is a sketch of a typical response curve for a silicon-based sensor (CCD chip).

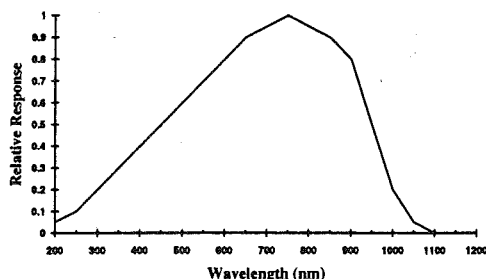


Figure 1. Response curve for a typical silicon-based CCD sensor (reproduced from Lake, 1994, p. 36).

3. THE IMAGE ACQUISITION SYSTEM REVISITED

In contrast to the BTG system, the AISAT system uses a commercial off-the-shelf, near infrared cold source¹, rather than a tungsten filament light source, to provide back-of-hand illumination. The IR cold source is a solid-state array of LEDs (light emitting diodes). A commercially available, low cost, monochrome CCD camera² fitted with an infrared filter³ is used to image the backs of hands. Our experiments showed that the cold source, which emits IR at a wavelength of $880 \text{ nm} \pm 25 \text{ nm}$, provides better contrast than ordinary tungsten filament bulbs. Figure 2 shows respectively: the emission curve for a tungsten filament light source and the emission curve for a typical LED, superimposed on the response curve for a typical CCD sensor (Figure 1). Clearly the system is exploiting only a very small window of the near IR spectrum. The window is not quite the one imposed by the IR cold source because the infrared filter, designed to transmit wavelengths greater than 900 nm, is not *ideal*. The transmission curve for the filter (Hoya RM90) was obtained using a spectrophotometer. The curve reveals that the filter has a small tail of transmittance down to about 750 nm (see Figure 3). The IR filter ensures that no visible light reaches the CCD sensor. The choice of off-the-shelf IR filters is rather limited. Kodak-Wratten produce five types of gelatine IR filters: 87, 87B, 87C, 88A, and 89B. All but the 87B transmit wavelengths in the 700 nm to 800 nm range. Hoya produces two glass IR filters: R72 and RM90. The former attenuates wavelengths less than 720 nm and the latter wavelengths less than 900 nm. Given the operating wavelength of the IR source, and the availability of filters from Australian suppliers, the Hoya RM90 was chosen.

Although the current imaging system retains the camera/IR-source/filter combination used in the original AISAT system (Mehnert et al., 1993, p. 5), it differs in four important respects:

- (i) the convex mirror assembly used to concentrate the wide-angle IR beam onto the back of a hand has been removed and replaced by diffusing paper over the IR source,
- (ii) the imaging unit is now enclosed so that no ambient IR radiation or external IR sources can reach the CCD sensor,
- (iii) the subject no longer presents the back of the hand to the camera by gripping a foam mould, rather the hand is presented as a clenched fist with the thumb covered by a piece of black card, and

¹ Model TC8245IRW, Burtle Industries Incorporated, Security Products Division, Lancaster, PA, USA

² Model OS-458, Mintron Enterprise Company Limited, Taiwan

³ Model RM90, Hoya Corporation, Japan

- (iv) images are captured at a higher spatial and radiometric resolution; now $640H \times 480V$ pixels and a grey-scale resolution of 8-bits per pixel (i.e. 256 shades of grey), as opposed to $320H \times 400V$ pixels and a grey-scale resolution of 7-bits per pixel (i.e. 128 shades of grey).

Figure 4 is a sketch of the imaging unit. A simple U-shaped docking frame is used to constrain the subject's hand. The docking frame and the base of the unit are painted with poster black, flat acrylic, scenic paint⁴ to minimise reflection of IR radiation from their surfaces. A simple *dimmer* switch is used to attenuate the intensity of the IR source; this is necessary because the source is actually an indoor IR security light and produces an intense, wide-angle beam. A monochrome frame-grabber⁵ is used to capture a video image of the back of a hand (see Figure 5) for computer processing. The sides and back of the imaging unit are completely closed. A cloth is draped over the top and front of the unit; this provides easy access to the camera/IR-source assembly, and allows a subject to easily position his/her hand in the docking frame.

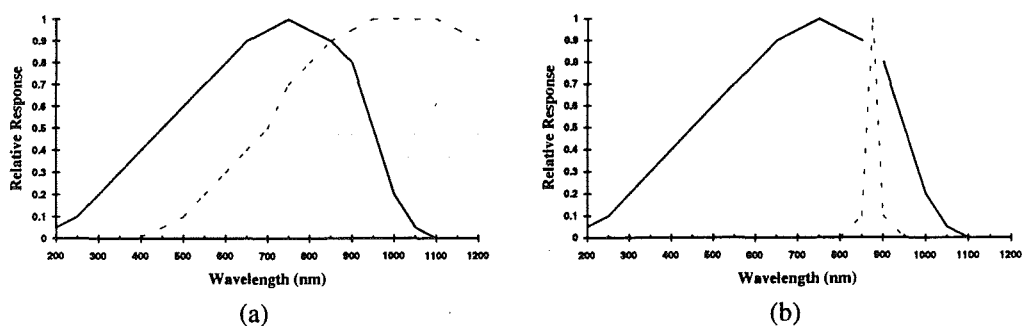


Figure 2. Response and emission curves (adapted from Lake, 1994, pp. 36-37)

- (a) Emission curve for a tungsten filament light source.
 (b) Emission curve for a typical LED.

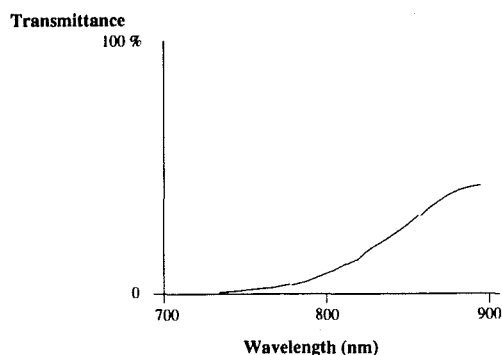


Figure 3. Transmission curve for the RM90 infrared filter.

⁴ Solver Paints, South Australia

⁵ Model DT2855 QuickCapture, Data Translation Incorporated, Marlboro, MA, USA

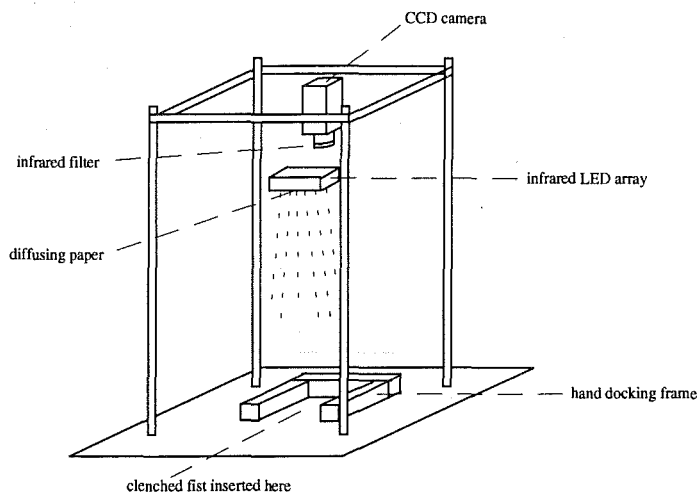


Figure 4. Schematic of the imaging unit.

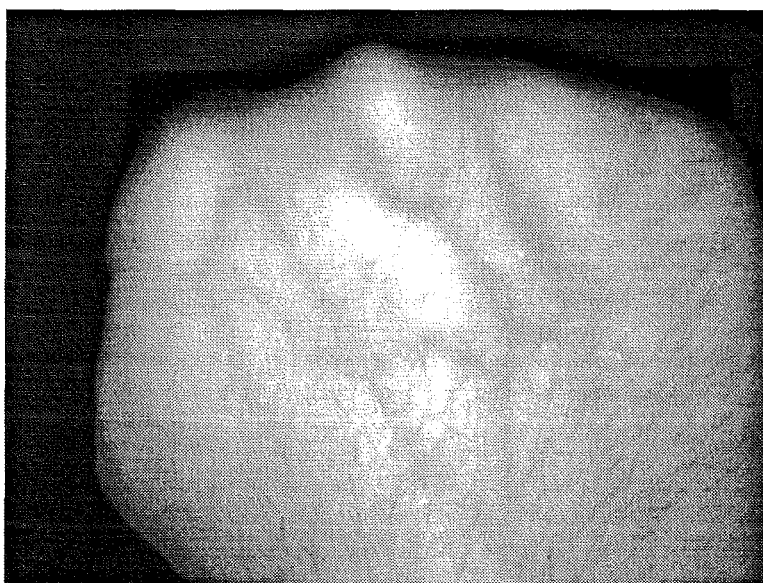


Figure 5. Frame-grabbed image of a male hand, 640H \times 480V pixels, 256 shades of grey.

4. SEGMENTATION AND CODING OF VEIN PATTERNS

In the original work of MacGregor and Welford (1991, 1992) vein patterns, traced onto acetate sheets directly from a monitor screen, were mapped onto a coarse hexagonal grid and reduced to a simplified representation for matching purposes. "The adequacy of this representation is questionable" (Mehnert, et al., 1993, p. 5). Indeed the BTG researchers have since proposed representing each vein "by a vector which has position and angle and can be regarded as a short straight line approximating a length of vein centreline" (Hawkes & Clayden, 1993, p. 1). We still submit that the digital skeleton (or medial axis) of the vein structure is a more faithful and robust representation than either of those proposed by the BTG.

Most recently the BTG researchers have used a local contrast enhancement function and thresholding to produce binary images (see Figure 6) of vein patterns from digital images of the backs of hands. They have claimed that "binary images processed in this way are sufficiently consistent that it is feasible to

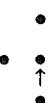
employ a two dimensional geometric matching method to decide if a presented image is of an imposter" (Hawkes & Clayden, 1993, p. 1).

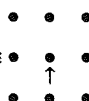
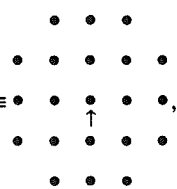






Figure 6. An example of a binary image of a left hand obtained by the BTG researchers (reproduced from Hawkes & Clayden, 1993).

We have devised an automatic segmentation and coding algorithm that effectively reduces a frame-grabbed image of the back of a hand to a medial axis representation. The medial axis is not only a faithful representation of the vein pattern but also an economical means of encoding it. It is the medial axis that is used in matching (after registration). The algorithm was developed using DIMPAL (Mehnert, 1994a) – a digital image processing and analysis language. The algorithm supersedes our original segmentation algorithm (Mehnert et al., 1993) which was prone to segmentation error when dealing with hairy hands; this is because the alternating sequential filter (ASF) used in the algorithm to attenuate noise⁶ had the propensity to merge clumps of hair. The new algorithm has an improved sensitivity to vein pattern structure and a much reduced sensitivity to noise – particularly hair. It is still based on Mathematical Morphology and retains many of the elements of its predecessor including: tophat transformation, opening, alternating sequential filtering, and gradient-based thresholding. Definitions of the binary and grey-scale morphological operators used, and the morphological gradient are given in Appendix A. A description of the algorithm follows:

Structuring elements (SEs)

Define $B_1 = \{(0,0), (0,1), (1,0), (0,-1), (-1,0)\}$, i.e. $B_1 \equiv$  •, where \uparrow denotes the origin,

$B_2 \equiv$  •, $C = B_1 \oplus B_2 \equiv$  •,

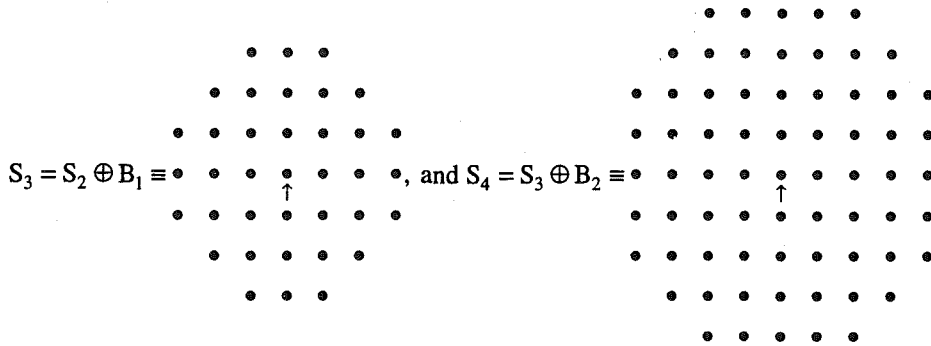
$L_1 \equiv$  •, $L_2 \equiv$  •, $L_3 \equiv$  •, and $L_4 \equiv$  •,

⁶ it was incorrectly stated that the filter removed thresholding artefacts

$$S_1 = B_1,$$

$$S_2 = S_1 \oplus B_2$$

$$= C,$$



1. Attenuate impulse noise and enhance contrast – Figure 7(a)

Apply a 3×3 moving average to the frame-grabbed image to attenuate impulse noise. Call this smoothed image f . Next apply the anamorphosis $f(x,y) \rightarrow [f(x,y)]^2$, to increase contrast, and linearly interpolate the result so that its range is the interval $[0,255]$. Call this new image f' .

2. Determine the domain of the hand – Figure 7(b)

The maximum value, $t \in [0,255]$, of the morphological gradient of f' is the threshold value that separates the foreground (hand) from the background:

$$t = \frac{1}{2} \left[\max_{(x,y)} (\mathcal{D}(f', B_1) - \mathcal{E}(f', B_1)) \right],$$

and the domain of the hand is the threshold set $D = \{(x,y) | f'(x,y) \geq t\}$. The maximum value of the gradient necessarily occurs at the edges of the hand and is close to zero outside of the domain of the hand.

3. Reduce the domain to obtain the working domain – Figure 7(c)

First an open-closing (opening followed by a closing) is performed to eliminate any thresholding artefacts and to fill in any holes in the domain:

$$D' = \mathcal{C}(\mathcal{O}(D, C), C).$$

Next, this domain is eroded to leave a subset of the interior of the hand, the working domain W :

$$W = \mathcal{E}(D', nC), \text{ where } nC = \underbrace{C \oplus C \oplus \dots \oplus C}_{(n-1) \text{ times}}$$

We use a value of $n = 13$ which approximates the erosion of the domain by a disk of radius 27 pixels. Alternatively, a distance map of D' could be generated and then thresholded (see Mehnert et al., 1993).

4. Remove hair, skin pores and other noise – Figure 7(d), Figure 8

Hair is essentially linear noise. Now grey-scale opening "can be visualised as the sliding of the SE along the underside of the brightness surface of the image. Wherever the SE is unable to penetrate, the surface is smoothed over" (Mehnert, 1994b, p. 70). The closing acts in the same manner but on the top of the brightness surface. Consequently for 4 independent closings using

the SEs $\{L_1, L_2, L_3, L_4\}$ a given strand of hair will admit at most one of the structuring elements – i.e. it will be attenuated by at least 3 of the closing operations. However only veins and areas of uniform brightness will admit all four structuring elements. Thus a maximum (analogous to an intersection) of independent closings is used to attenuate hair:

$$f'' = \max_{i=1}^4 \{ \mathcal{C}(f', L_i) \},$$

In a similar fashion a minimum (analogous to an intersection) of independent openings,

$$f''' = \min_{i=1}^4 \{ \mathcal{O}(f'', L_i) \},$$

attenuates any positive thin linear structures, e.g. ridges between skin pores, and small artefacts induced by specular reflection. (Note: operations are restricted to the working domain, W).

5. Normalise the background – Figure 7(e),(f)

The back of a hand is a curved surface and hence the IR illumination across it is not uniform. To correct for this the brightness surface must be estimated and then *subtracted out* – background normalisation. This is achieved by closing f''' by an octagon sufficiently large so that it will not fit into any vein structure. Only the background remains. By subtracting f''' from this closing (on the working domain, W), called *tophat* transformation, only the vein structure is retained (once again we use $n = 13$):

$$g = \mathcal{C}(f''', nC) - f'''.$$

6. Threshold out the vein pattern – Figure 7(g)

Once again, the morphological gradient is used to obtain a threshold value; this time a value s that separates the vein pattern from the background:

$$s = \frac{1}{2} \left[\max_{(x,y)} \{ \mathcal{D}(g, B_1) - \mathcal{E}(g, B_1) \} \right],$$

and the vein pattern is the threshold set $V = \{(x, y) | g(x, y) \geq s\}$.

7. Remove artefacts, fill holes – Figure 7(h)

A binary alternating sequential filter, employing structuring elements approximating disks of increasing size, is used to remove any threshold artefacts, and to fill small holes in the vein structure:

$$V' = \Psi_4 \Psi_3 \Psi_2 \Psi_1(V), \text{ where } \Psi_i(A) = \mathcal{O}(\mathcal{C}(A, S_i), S_i).$$

8. Thin the pattern down to its medial axis – Figure 9

The binary vein pattern is thinned to its medial axis representation. The thinning algorithm used is a modification of the well known Zhang and Suen (1984) algorithm. The modification, devised by Sossa (1989), is a single post-thinning pass through the image that removes redundant pixels to ensure that the medial axis has single pixel thickness.

9. Prune the medial axis – Figure 10, Figure 11

The thinned image is scanned and all skeletal endpoints identified. From a given endpoint the thinned image is tracked until either another endpoint is reached – in which case a length of vein has been tracked – or an intersection point is reached – in which case a branch was tracked. Branches of length less than $\beta = 40$ pixels, and veins of length less than $\alpha = 60$ pixels are removed. This is done for each endpoint independently and the whole process is repeated until convergence (when no more pruning can be done). Spurious segments induced by shadows and large clumps of hair are eliminated whilst the dominant veins are retained.

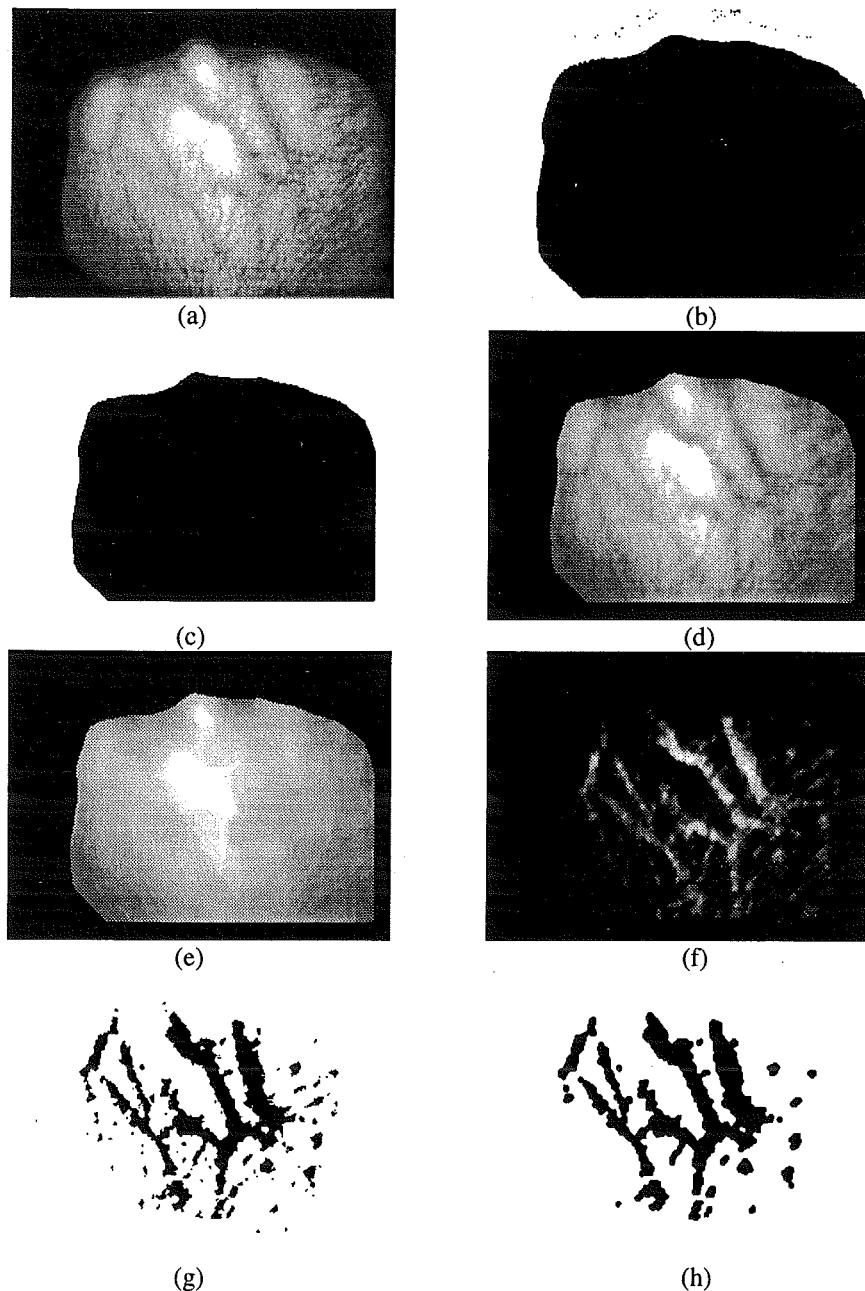


Figure 7. Segmentation of the vein pattern.

- (a) Figure 5 after mean filtering and contrast enhancement;
- (b) Domain obtained from the gradient-based thresholding of (a);
- (c) Open-closing of (b) by a small octagon, followed by an erosion by a large octagon (yielding the *working domain*);
- (d) Filtering of (a), on the working domain, to remove hair and other noise;
- (e) Closing of (d) by an octagon larger than the width of the largest vein – estimate of the background brightness surface;
- (f) Tophat transform: (e) subtract (d) – background normalisation;
- (g) Vein pattern, after registration, obtained from the gradient-based thresholding of (f)
- (h) ASF applied to (g).

At present the vein pattern signature images are coded using the following run-length encoding scheme:

The most significant bit of each byte in a run-length encoded signature image records a pixel value of either 1 (part of medial axis) or 0. The remaining 7 bits represent a repetition count in the interval [1,128]. The process of decoding a run-length encoded signature image thus involves reading the code byte and duplicating the value indicated by the most significant bit the number of times dictated by the remaining bits. This simple compression strategy reduces a 300 Kb frame buffer ($640H \times 480V \times 8$ bits) to on average 3.5Kb for a signature image ($\approx 1.2\%$ of original size).

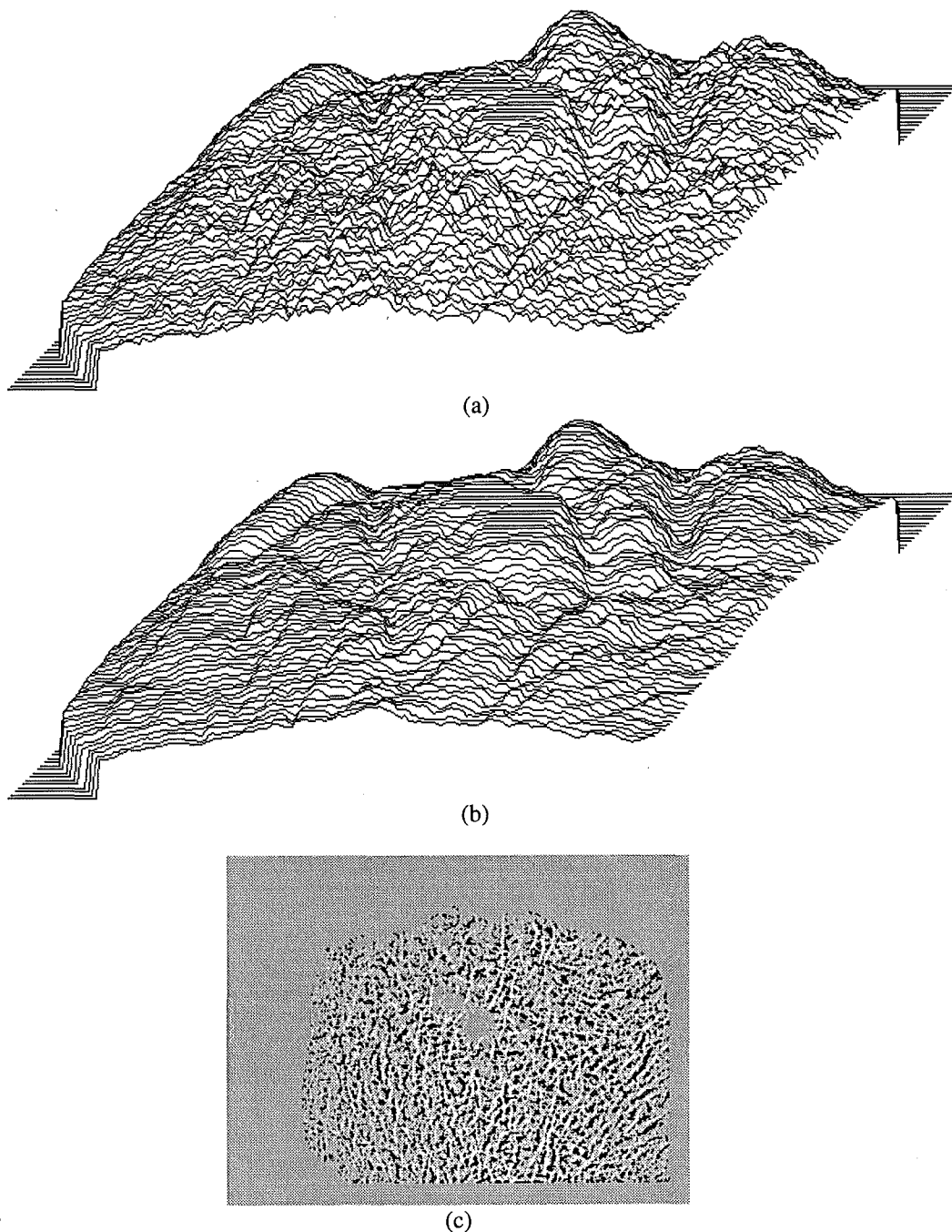


Figure 8. Performance of the custom noise filter of step 4 of the segmentation algorithm.

(a) Figure 7(a) rendered as a 3D surface;

(b) Figure 7(d) rendered as a 3D surface;

(c) Histogram equalisation of the difference between Figure 7(a) and Figure 7(d) showing the noise removed by the custom filter.

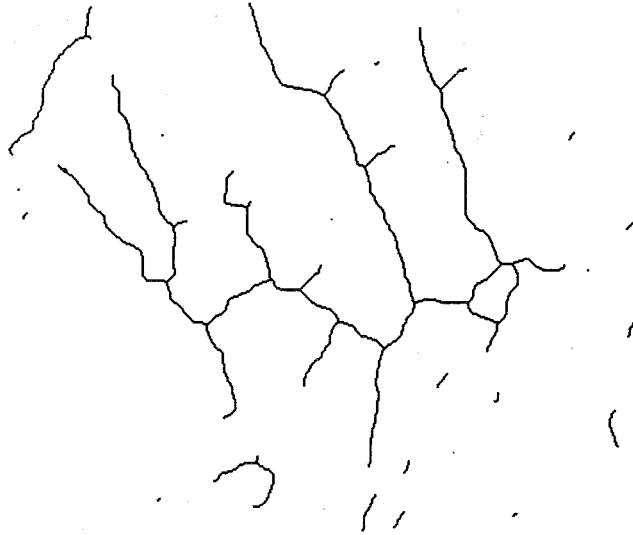


Figure 9. Medial axis representation of Figure 7(h).

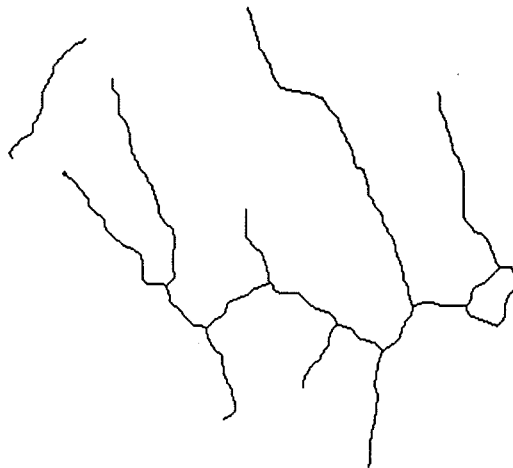


Figure 10. Figure 9 after pruning.

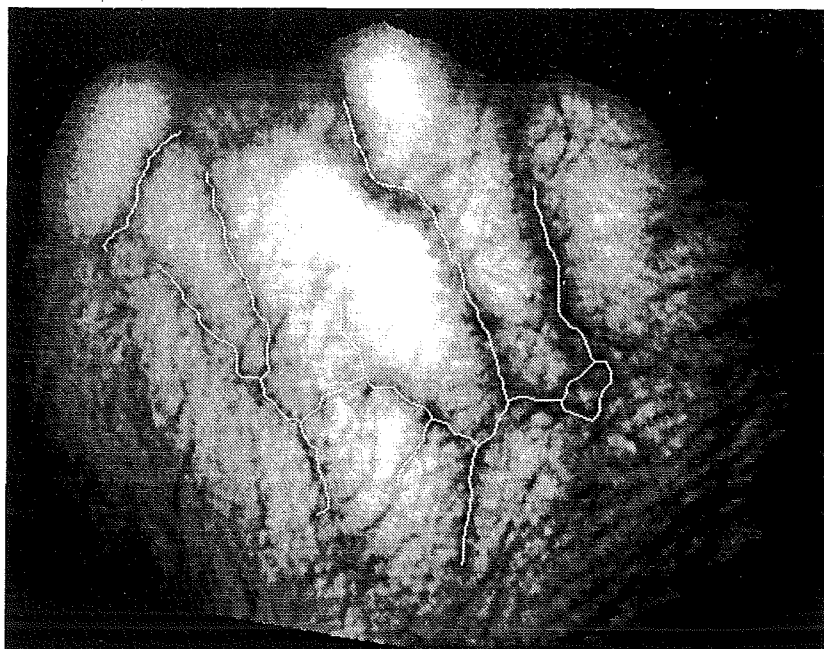


Figure 11. Figure 10 superimposed on the original image (histogram equalised and registered) depicted in Figure 5.

5. VEIN SIGNATURE REGISTRATION

To match a vein signature against one or more library signatures initial registration is necessary to correct for slight variations in a subject's placement of their hand at the time of capture. MacGregor and Welford (1991,1992) used the outline of the hand, in particular that of the knuckles and the side of the hand opposite the thumb, to facilitate manual registration. Our research has shown that this approach is not suitable for automatic registration, particularly when employing the U-shaped docking frame, because

- (i) shadows can obscure the outline of the hand,
- (ii) of the variability associated with hand placement (when no docking frame is used), and
- (iii) the outline of the hand can be distorted by the deformation of the side of the hand pressed against the docking frame.

Registration

Our original approach to rotation correction involved calculating the orientation of the *principal axes of area* about the centroid (called *principal centroidal axes*) for the *working domain*, obtained in step 3 of the segmentation algorithm, viz:

$$\tan 2\theta = -\frac{2P_{xy}}{I_x - I_y},$$

where $I_x = \int y^2 dA$, $I_y = \int x^2 dA$, $P_{xy} = \int xy dA$ are the moments and product of inertia, about the centroid, of the area A ; i.e. the *working domain* W . However for a sequence of images obtained by repositioning the hand in the docking frame, the vein signatures, in some instances, exhibited enough rotational error to render simple correlation matching of two signatures useless. Our current approach to registration is to first obtain a reference axis (position vector) defined by the centroid of the *working domain* of the hand and the midpoint of the last row (at the wrist) of this domain. The centroid defines the origin of the position vector, and together with the midpoint of the last row, defines its direction. Registration involves translating this position vector to the centre of the image buffer (640H \times 480V pixels), i.e. coordinates (320, 240), and then rotating it so that it is perpendicular to the horizontal. Registration takes place immediately after step 6 of the segmentation algorithm. Our research has shown that this registration process is robust in correcting for rotation and vertical translation. However vein signatures still exhibit

some horizontal positional noise (see Figure 12). This is probably due to deformation of the side of the hand pressed against the docking frame, and to variation in the positioning of the card used to mask the thumb. Fortunately this variation can be accounted for in the matching strategy.

It is interesting to note that the BTG have proposed a similar registration scheme, though one which is considerably more computationally expensive than ours. They have suggested that "automatic alignment can be achieved by scanning the image [see Figure 6] with a coarse scan and analysing samples of the veins" (Hawkes & Clayden, 1993, p. 1). This analysis involves: approximating lengths of vein by vectors, choosing the approximately vertical ones to assist with horizontal alignment, the approximately horizontal ones for vertical alignment, and using the others to assist in determining a rotation correction.

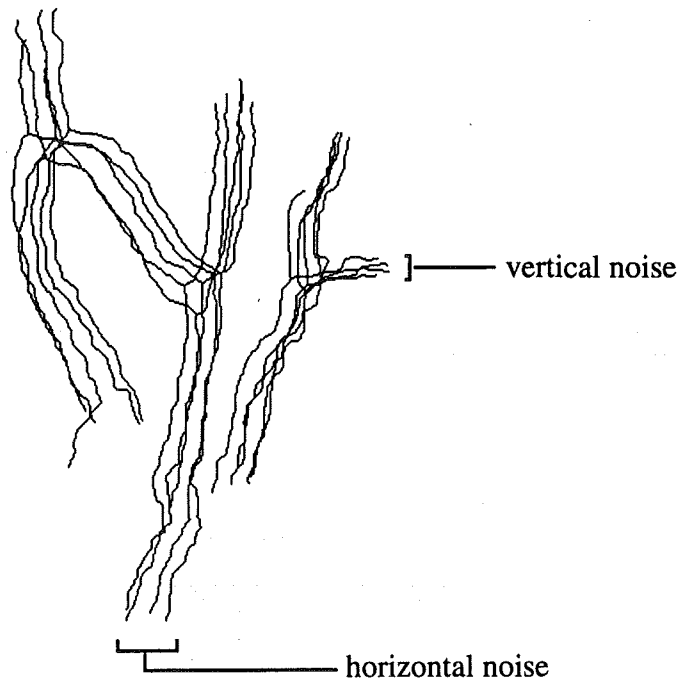


Figure 12. An overlay of 5 signatures, after registration, obtained from 5 repositionings of the same hand in the docking frame. Significant horizontal positional noise is still evident after registration (vertical positional noise is comparatively negligible).

6. VEIN PATTERN MATCHING

A back-of-hand vein pattern biometric system must be able to positively identify a person by matching a newly acquired vein signature against a reference signature (library template) stored in a database or encoded on a smart-card. A simple pixel by pixel comparison of two signatures is not viable for two main reasons:

- (i) subcutaneous blood vessels have some freedom to move because they are surrounded by soft tissue and their position is thus influenced by factors such as the degree of flexing of the hand, and
- (ii) they exhibit varying degrees of dilation depending on the person's physiological state which is influenced by – amongst other factors – physical activity and the ambient temperature.

6.1. Grid based matching

MacGregor and Welford (1991,1992) mapped vein pattern networks, by hand, onto a coarse hexagonal grid (see Figure 13). "The grid resolution was selected to provide an adequate representation of the vein-tree, but at the same time its size matches the inherent noise associated with the positional

information of the vein structure" (1992, p. 54). A hexagonal grid was chosen in preference to a square grid because it supports higher connectivity and matches the topology of the vein structure reasonably well. The representation permitted the construction of a connectivity matrix for each vein pattern describing the connectivity of the grid of hexagons. Each element of the matrix is a n -tuple comprising the coordinates of a hexagon within the grid and the connections between the hexagon and each of its six neighbours (indicated by a 1 or 0). The ratio of the number of common connections to the total number of vein connections for all hexagons then provides a measure of the similarity between two connectivity matrices. MacGregor and Welford (1992) obtained the similarity values between the vein patterns from 20 different hands. All similarity measures for different hands were less than 0.45. They also performed a *blind* test in which 5 independently acquired vein patterns were compared against the library of 20. Two of these test patterns were obtained from individuals whose signatures were already in the library. Although there were no mismatches, in one case, the similarity value for two different images of the same hand yielded an unacceptably low 0.228. This result is not surprising; we have observed that the mapping procedure can produce markedly different representations of the vein structure depending on the exact placement of the hexagonal grid over the hand image.

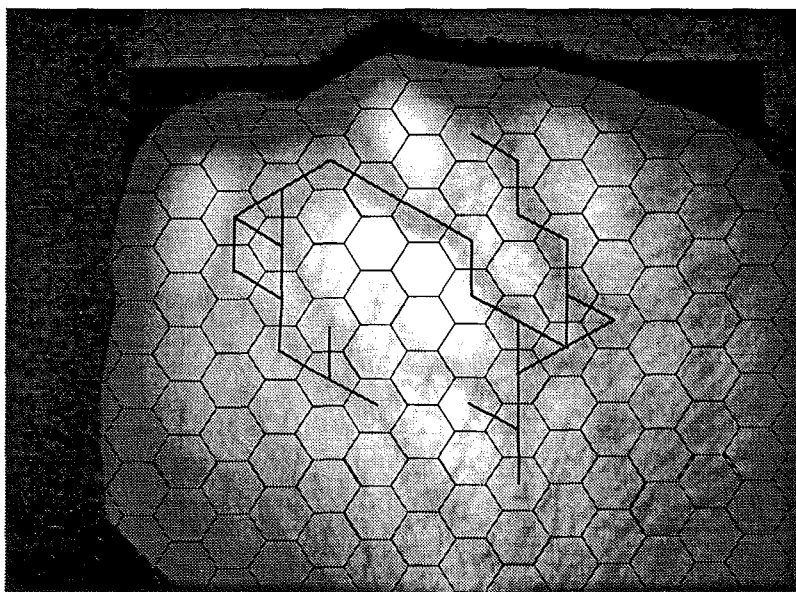


Figure 13. Mapping the vein pattern onto a coarse hexagonal grid. (In this case the image is the histogram equalisation of Figure 5).

6.2. Matching of vein signatures using constrained sequential correlation

Our approach to matching is to compare medial axis representations obtained from the segmentation and coding algorithm (after registration) using what we have termed *constrained sequential correlation*. The method is a variation on the traditional correlation methods used for template matching. The reference or library signature is first dilated by an octagonal structuring element, nC (approximating a disk). The size of this structuring element ($n = 4$) was chosen based on observations of the inherent positional noise exhibited by a length of medial axis from several signatures of the same hand. The test signature is then superimposed on this reference buffer and the percentage of pixels contained within the buffer determined. To account for the horizontal translation error still evident after registration the test signature is sequentially translated horizontally and compared against the reference buffer. The horizontal translations are constrained to ± 30 pixels. The highest match percentage in this interval is deemed to be the measure of *forward* similarity between the test and library signature. As the proportion of vein pixels in the test signature can be small relative to the library signature the preceding process is reversed; i.e. the test signature is dilated and the reference signature is sequentially correlated with it until the maximum measure of *reverse* similarity is obtained. For the test signature to match the library signature both the forward and reverse percentages must be high. As an experiment we captured 5 infrared back-of-hand images from each of 20 adults. Each individual was required to reposition his/her hand in the docking

frame between captures. This group comprised 3 females and 17 males. It included the following racial groups: Caucasian, Indian, and Oriental. In addition, for two of the individuals, another set of 5 observations were included; these had been captured several weeks earlier. All of the images were processed and registered. For each set of 5 signatures a library template was constructed from the last 3 signatures (chronologically speaking). Construction of this template involved:

Construction of the library template

- (i) dilating, thinning, and pruning the third signature and storing the result in the library template memory;
- (ii) horizontally translating the fourth signature so as to achieve the highest correlation with the library template, taking the union of the translated signature and the library signature, dilating, thinning, and pruning the result and storing this in the library template memory (overwriting the previous result); and
- (iii) translating the fifth signature so as to achieve the highest correlation with the library template, taking the union of the translated signature and library signature, dilating, thinning, and pruning the result and storing this in the library template memory (overwriting the previous result) – see Figures 14 and 15.

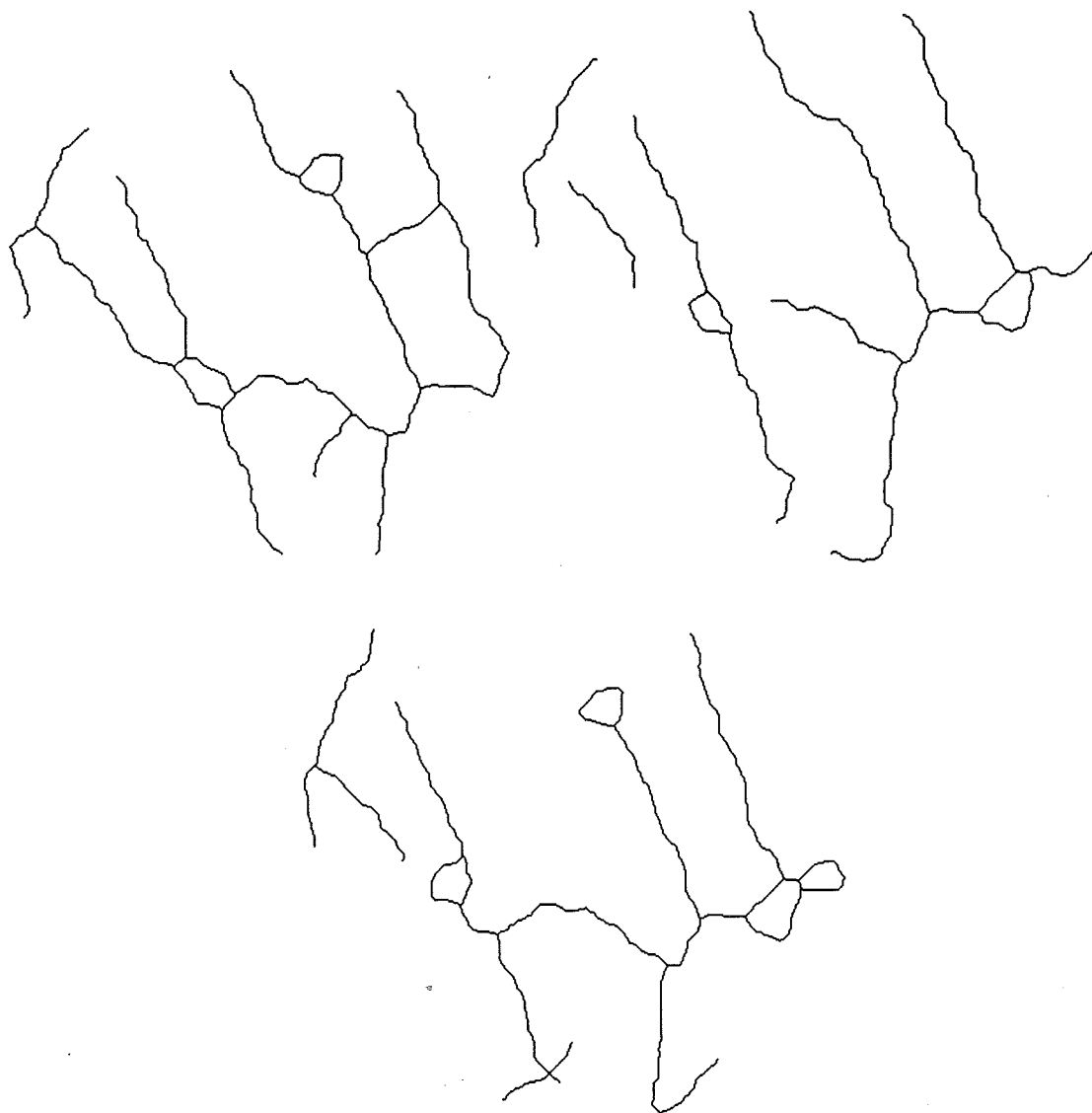


Figure 14. The last three signatures obtained from the individual whose first signature is depicted in Figure 10.

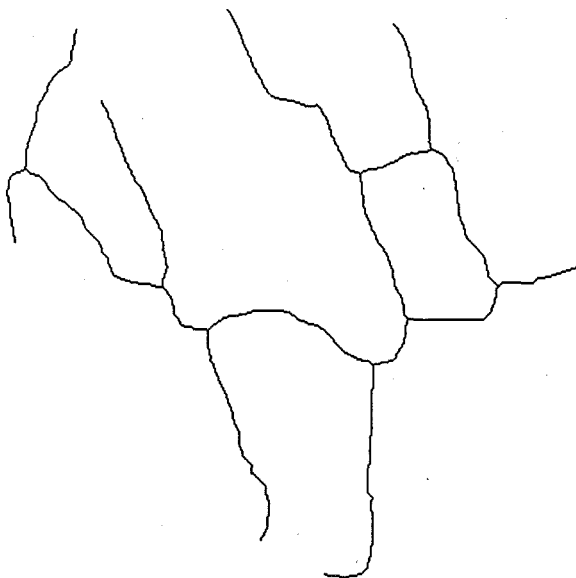
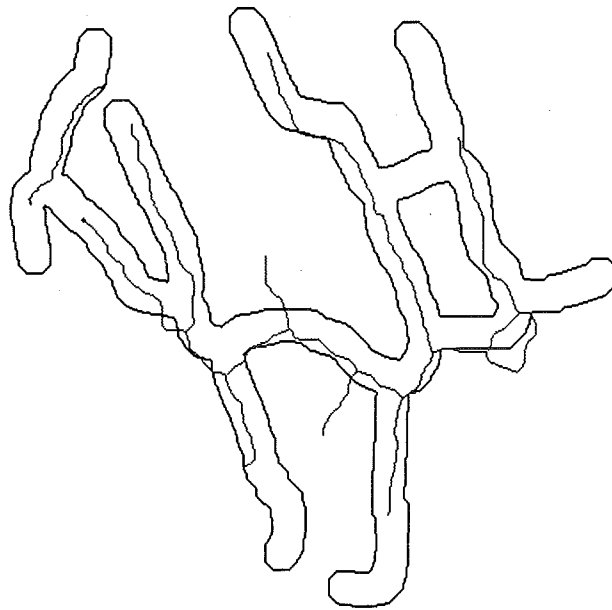


Figure 15. Library template constructed from the 3 signatures shown in Figure 14.

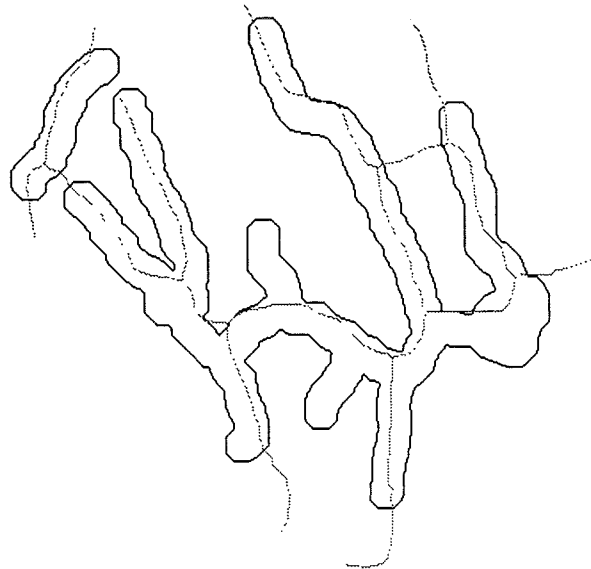
The construction process can of course accommodate any number of *training* signatures. Figure 16 demonstrates the matching process for the signature shown in Figure 10 and the library template shown in Figure 15. Table 1 shows the results of cross-matching the first signature (not used in the construction of a library template), from each set of 5, with each of the library templates. Similarly Table 2 shows the results of cross-matching the second signature (also not used in the construction of a library template), from each set of 5, with each of the library templates. By the very nature of its construction a library template contains more information than any single signature. Hence the minimum acceptable percentage for a forward match should be higher than that for a reverse match. Setting the minimum forward and reverse percentages to 75% and 60% respectively for positive identification, all but signatures 3 and 17 are identified in Table 1, and all but signature 4 are identified in Table 2. This constitutes a FRR of 7.5% (based on 20 individuals). Moreover because there are no mismatches the FAR is 0%. Lowering the minimum forward percentage to 70% reduces the FRR to 5% without affecting the FAR. Signature 17 of Table 1 is an unusual case. The signature has a 66% forward match with its own library template and a 70% forward match with library template 21 (see Figure 17). Clearly the reason for the poor match with its own library template is that the signature and its template are not correctly vertically registered. Figure 18 shows the first captured image of individual 21's hand, and the 5 images captured of individual 17's hand. Unfortunately the docking frame is about 1 cm too low and this allows individuals with large hands the freedom to rotate the knuckles over the front of the docking frame. This is exactly the case for individual 17; one can clearly see in the first image that the knuckles are very close to the top of the picture compared to the other 4 images. To make matters worse in the fourth image the hand is not firmly pressed against the top of the docking frame; and as a result the library template, because it is constructed from the last 3 images, retains some vertical translation error. Consequently the first signature of individual 17 fails to match against library template 17 even though the person's second signature does. What is remarkable though is that the first signature of individual 17 achieves a 70% forward match with individual 21's library template. This level of match is attained for a horizontal translation of 29 pixels. When the sequential correlation matching algorithm is constrained to ± 20 pixels the degree of forward match is reduced to 60%, and for ± 15 pixels it is only 50%. Clearly the inherent horizontal registration problem of the current imaging system needs to be addressed.

Templates 7 and 8 are actually from the same individual. They were obtained from two sets of 5 images captured several weeks apart (and under slightly different lighting conditions). Similarly templates 13 and 14 belong to another single individual. Test signatures 7 and 8 of Table 1 and 7 and 8 of Table 2 match both template 7 and template 8. Test signature 14 of Table 1 and 14 of Table 2 match both template 13 and template 14. However test signature 13 of Table 1 and 13 of Table 2 only match template

13. Their respective reverse match percentages with template 14 are both very high: 80% and 83%. This indicates that the set of signatures used to construct template 14 contain less detail than those used to construct template 13. Clearly a library template needs to be constructed from a series of images captured under optimal conditions. For instance an individual being enrolled in the system might be required to repeatedly squeeze, say, a rubber ball just prior to image capture so that the blood vessels are dilated and thus well defined.



83% forward match



75% reverse match

Figure 16. Forward and reverse matches for signature 5 of Table 1 (shown in Figure 10) against library template 5 (shown in Figure 15).

Table 1. Forward/reverse template match percentages for the first signature obtained from 20 people.

Signature	Library Template																					
	1	2	3	4	5	6	7	8	9	10	11	12	13	14	15	16	17	18	19	20	21	22
1	91	37	37	27	55	42	45	51	53	53	39	49	59	66	59	40	42	61	52	67	44	37
	78	26	22	28	26	28	31	26	40	28	25	48	30	35	31	18	29	28	26	27	26	24
2	29	78	35	33	45	33	38	41	28	37	43	34	49	41	44	48	32	52	29	48	32	36
	45	97	37	60	36	39	43	36	42	38	48	55	47	49	38	37	38	42	29	36	37	44
3	29	43	73	19	40	26	27	28	46	29	30	31	49	35	32	31	41	46	31	42	34	34
	41	60	78	33	34	33	30	30	64	32	34	51	42	31	29	27	47	41	28	31	40	41
4	41	44	46	91	38	40	39	38	33	44	26	33	50	37	56	44	47	51	43	47	30	49
	33	30	25	85	16	22	24	19	22	27	17	34	21	21	29	19	27	21	22	18	18	29
5	28	30	33	24	83	23	31	27	30	38	24	22	35	33	33	36	28	39	34	48	25	44
	48	40	41	52	75	33	42	30	42	45	31	38	36	39	33	34	39	33	38	39	31	58
6	28	38	45	25	46	98	45	25	46	32	31	30	54	47	41	46	38	37	40	63	36	36
	34	43	39	41	31	97	43	21	55	29	30	40	41	40	35	32	38	27	32	39	33	36
7	45	26	33	17	38	40	82	89	24	28	23	22	43	47	40	29	21	47	47	56	47	30
	59	32	32	30	26	43	86	76	25	23	23	30	34	45	34	22	24	33	38	35	44	33
8	44	27	33	14	31	28	79	86	23	29	34	31	41	48	43	41	33	43	45	42	44	25
	53	28	30	19	20	23	78	68	21	23	30	45	30	38	33	27	30	25	36	25	38	22
9	43	27	43	31	33	43	30	29	77	39	41	29	50	41	43	42	32	47	54	54	55	36
	57	31	37	47	24	46	35	26	89	33	38	43	39	34	37	31	34	32	46	33	53	35
10	28	34	31	29	39	33	28	28	34	96	24	35	46	38	50	53	26	46	45	50	41	47
	38	41	27	45	28	33	31	23	40	81	23	50	35	35	37	39	27	31	35	31	38	42
11	26	44	28	16	41	20	26	33	39	32	89	28	49	43	43	35	37	47	39	57	34	34
	39	52	28	27	32	21	28	29	50	34	94	45	41	45	42	30	42	38	39	41	37	39
12	61	41	42	30	45	37	30	53	44	35	36	100	60	58	60	44	47	58	46	64	39	54
	51	32	27	30	21	24	21	29	35	18	22	96	30	37	32	23	31	26	26	28	26	38
13	22	29	31	23	41	39	30	28	39	34	37	31	93	64	43	38	32	43	43	44	32	38
	42	43	37	48	38	53	42	32	61	42	48	65	95	80	47	37	45	40	48	40	43	54
14	26	41	28	30	52	45	38	37	44	38	44	44	100	91	46	38	26	47	49	50	38	48
	31	45	27	41	34	44	38	29	50	34	39	60	73	81	36	28	27	27	37	29	38	49
15	29	34	36	18	31	48	30	34	28	45	29	38	44	38	95	41	33	43	49	56	29	37
	40	44	38	32	23	56	35	30	39	41	28	58	36	32	83	31	39	32	47	41	30	43
16	21	34	27	19	33	28	24	33	30	40	29	25	37	31	31	89	23	40	25	43	26	28
	36	53	34	38	32	37	33	34	46	50	36	44	40	39	33	87	32	36	30	35	35	36
17	26	35	40	25	59	41	32	27	39	20	42	29	42	47	34	32	66	36	44	51	70	30
	28	35	36	39	38	39	33	21	43	18	35	42	33	38	27	20	62	23	35	28	59	28
18	26	29	27	18	36	21	35	33	32	36	35	24	39	39	45	32	30	89	38	40	24	33
	48	50	36	40	35	35	47	39	54	45	46	48	42	47	50	33	42	82	43	36	33	47
19	30	24	30	28	39	31	41	40	32	52	37	30	49	45	42	30	35	38	86	52	43	31
	52	41	43	59	37	42	56	44	54	67	52	67	55	61	47	30	48	37	97	47	58	45
20	26	41	24	18	38	43	29	38	27	28	45	21	39	37	51	41	25	42	25	98	29	31
	43	54	27	35	31	53	33	35	38	29	47	39	36	42	50	36	34	34	24	73	33	41
21	31	39	32	18	38	32	43	41	42	49	34	30	47	56	35	43	32	42	50	60	89	30
	50	52	33	33	33	37	57	43	55	52	35	53	44	57	33	37	35	34	49	46	100	37
22	23	36	32	30	46	35	26	28	38	41	34	35	46	38	44	47	34	51	37	47	28	89
	33	45	35	53	35	43	29	28	52	41	35	51	38	36	42	40	39	40	33	33	31	100

Notes.

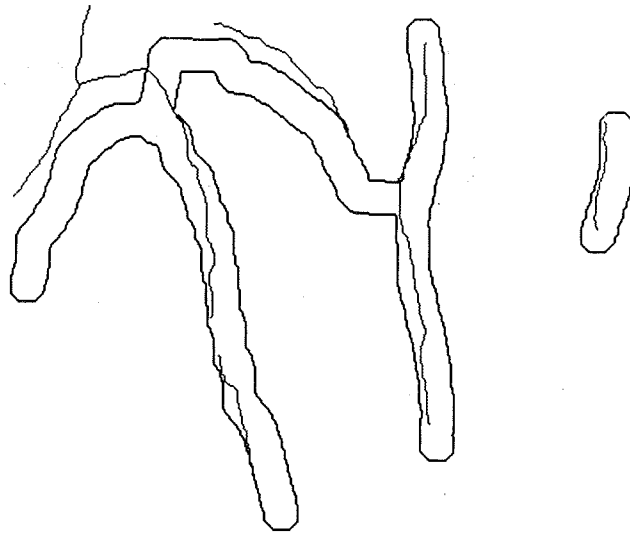
- (i) Signatures/templates 7 and 8 are from one individual, and signatures/templates 13 and 14 belong to another single individual (data were collected several weeks apart).
- (ii) Upper cell entry indicates the forward match percentage and the lower cell entry indicates the reverse match percentage.
- (iii) A shaded cell indicates a forward match of 75% or greater and a reverse match of 60% or greater.
- (iv) Boldly outlined cells are unusual observations.

Table 2. Forward/reverse template match percentages for the second signature obtained from 20 people.

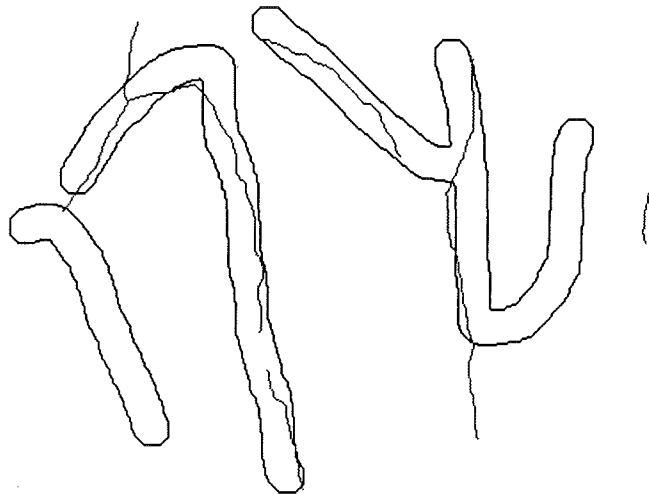
Signature	Library Template																					
	1	2	3	4	5	6	7	8	9	10	11	12	13	14	15	16	17	18	19	20	21	22
1	94	30	34	47	42	44	49	47	65	53	35	53	57	73	45	56	35	65	54	64	47	38
	69	19	16	37	16	28	30	23	39	26	18	39	22	32	23	22	20	26	22	22	24	19
2	31	82	36	36	45	33	35	36	28	38	43	36	50	44	44	50	34	54	30	48	31	37
	43	97	37	63	33	38	38	30	39	36	47	54	43	47	38	37	38	41	28	34	34	43
3	29	36	92	24	38	29	30	33	44	25	27	27	38	32	36	34	30	41	31	34	31	31
	43	47	95	45	32	37	33	30	57	27	32	42	35	33	31	29	36	32	30	28	37	38
4	30	49	57	72	44	48	24	36	38	58	31	45	49	33	50	65	68	50	43	53	39	51
	21	28	25	57	16	25	13	14	23	27	17	33	17	16	22	26	33	18	18	16	19	25
5	28	30	33	24	83	23	31	27	30	38	24	22	35	33	33	36	28	39	34	48	25	44
	48	40	41	52	75	33	42	30	42	45	31	38	36	39	33	34	39	33	38	30	31	58
6	32	38	48	28	45	99	43	26	42	35	30	29	55	48	50	50	34	39	41	56	37	36
	40	40	41	44	29	98	41	23	49	32	29	37	41	40	40	32	33	26	32	35	34	35
7	45	29	25	23	46	46	90	87	32	37	18	22	55	58	46	32	28	40	55	49	50	34
	49	24	19	35	25	39	75	37	27	26	17	25	34	45	29	19	21	21	36	23	41	27
8	46	29	34	19	42	46	93	94	32	37	21	25	57	61	49	31	25	40	58	54	52	29
	47	24	28	24	26	39	77	63	26	25	17	27	34	43	31	18	20	22	37	25	39	23
9	39	36	50	29	39	51	29	30	95	35	50	37	63	53	54	55	39	51	53	52	57	40
	45	36	38	41	25	44	27	20	93	27	39	43	42	38	41	32	34	31	38	26	47	34
10	40	30	25	29	47	37	29	33	27	90	24	27	35	30	41	52	23	42	50	44	36	34
	54	42	26	55	31	38	32	26	38	86	24	43	31	34	39	41	25	35	41	30	36	39
11	29	45	38	17	50	24	22	31	30	28	89	27	51	37	49	42	38	37	31	50	25	27
	37	45	33	24	32	24	21	22	33	23	82	38	38	37	40	27	38	25	27	30	24	26
12	45	48	41	28	44	41	30	34	48	48	35	97	61	59	56	57	31	60	45	60	40	54
	41	40	25	33	22	33	24	20	39	31	24	95	33	40	32	31	21	29	26	27	27	40
13	21	31	29	23	45	38	34	30	40	36	39	31	97	68	42	40	26	49	46	45	32	36
	38	47	36	46	40	51	48	33	63	43	51	67	94	83	45	37	33	45	47	38	42	49
14	27	33	30	33	55	43	42	41	45	39	41	41	96	92	45	39	31	44	55	51	44	40
	37	40	30	46	39	46	42	33	54	34	39	63	76	85	37	30	34	32	45	30	43	46
15	27	30	38	19	28	54	30	35	28	40	29	34	43	34	93	37	34	38	44	54	28	36
	40	42	40	34	23	62	35	32	35	38	33	55	39	32	86	33	43	30	46	41	32	41
16	20	32	27	20	35	30	25	26	29	41	33	27	37	35	31	99	32	36	25	44	22	33
	37	47	33	40	32	43	31	28	46	49	41	49	38	42	34	93	41	33	30	33	28	48
17	32	31	38	28	54	40	30	26	34	24	47	30	45	43	34	29	78	35	54	45	59	26
	37	35	36	48	38	44	31	22	39	22	40	45	38	42	27	22	78	25	42	30	57	25
18	29	40	35	19	36	26	24	28	35	34	30	22	38	32	43	28	24	85	36	45	28	28
	47	54	35	34	31	31	31	27	51	36	32	36	39	31	39	25	30	70	36	37	34	33
19	29	21	32	30	34	28	36	35	33	52	37	29	45	39	39	29	36	43	95	43	44	33
	44	29	34	54	28	36	47	37	46	60	43	55	44	44	40	27	45	37	95	35	51	44
20	39	41	37	21	43	52	36	43	26	35	45	40	36	45	62	34	36	41	36	99	40	36
	46	44	29	38	28	50	32	32	29	29	39	50	27	37	46	21	33	27	28	61	36	37
21	33	43	37	19	38	33	42	40	43	49	35	32	48	59	36	43	37	38	51	59	92	32
	50	49	37	35	30	37	49	37	49	48	33	53	41	52	30	34	37	28	44	41	93	36
22	23	32	35	27	45	34	25	29	44	39	36	36	50	38	48	42	36	55	34	49	30	94
	31	38	33	42	32	35	25	24	52	38	34	52	40	32	43	33	37	41	30	30	31	97

Notes.

- (i) Signatures/templates 7 and 8 are from one individual, and signatures/templates 13 and 14 belong to another single individual (data were collected several weeks apart).
- (ii) Upper cell entry indicates the forward match percentage and the lower cell entry indicates the reverse match percentage.
- (iii) A shaded cell indicates a forward match of 75% or greater and a reverse match of 60% or greater.
- (iv) Boldly outlined cells are unusual observations.



66% forward match



70% forward match

Figure 17. Forward matches for signature 17 of Table 1 against library templates 17 and 21 respectively.

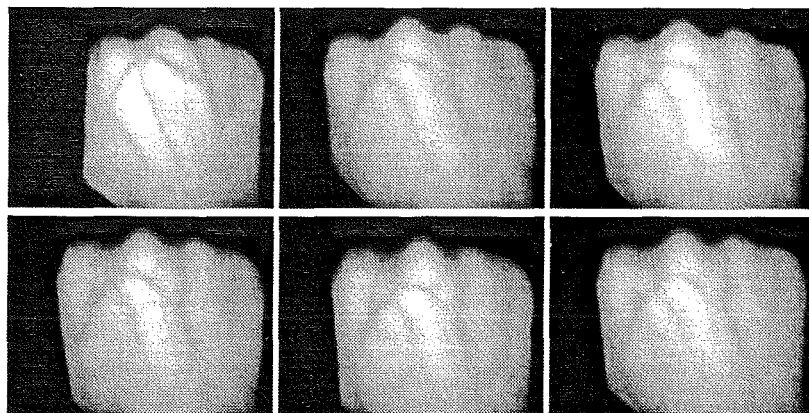


Figure 18. From left to right, first hand image of individual 21, then hand images 1 to 5 of individual 17.

6.3. Matching of vein signatures using fuzzy relaxation

The classical approach to matching images is to use correlation and sequential matching (Gottesfeld Brown, 1992). Correlation matching methods include: correlation coefficients, sum of absolute differences in intensity, sequential thresholding, sign change criteria, and region overlap criteria (such as the constrained sequential correlation matching algorithm just described). Infrared back-of-hand images of a single hand, both raw and processed, exhibit marked variability (e.g. Figure 14). This is primarily due to specular reflection, clumping of hair, the extent of venous engorgement, the mobility of subcutaneous veins, and registration error. These factors collectively diminish the accuracy of correlation matching. Signature 17 of Table 1 is a case in point. An alternative approach to sequential correlation for matching signatures is to use a graph theoretic approach. "Graph theoretic . . . matching methods have the advantage that they are capable of dealing with the problems caused by differences in imaging geometries (location of sensors, viewing angles, etc.) noise, and the limitations of the image segmentation algorithms better than template matching methods" (Ranganath & Chipman, 1992, p. 631). In relation to vein signature images variability is due to segmentation and registration error. Generally speaking 5 types of segmentation error are possible:

- (i) *mismeasured attributes*: the presence of noise in an image can affect the quantitative measurement of objects in the segmented image thus leading to misclassification; e.g. a length of vein in one signature image might appear longer or shorter than in another signature image of the same hand;
- (ii) *missing objects*: an object not clearly visible due to glare, shadows, or occlusion is not represented in the segmented image;
- (iii) *false objects*: extraneous marks or shadows appear as objects in the segmented image;
- (iv) *fragmented objects (oversegmentation)*: noise-induced spurious edges fragment an object into more than one region in the segmented image;
- (v) *merged objects (undersegmentation)*: two or more objects are merged to become one region in the segmented image as a result of noise-induced blurred edges.

The graph theoretic methods that address these segmentation errors are classified as structural matching techniques. They include dynamic programming using edge-image graphs (Fukunaga, 1991), and fuzzy relaxation using association graphs (Ranganath & Chipman, 1992). An edge-image graph represents objects or regions in an image by nodes and their relationships by arcs. For example a vein signature might be represented by a series of line segments joining endpoints and junctions (see Figure 19). An edge-image graph could then be constructed by assigning nodes to the midpoints of the line segments and defining an arc as the distance or angle between nodes. When matching pairs of images (e.g. vein

signature against library template) the association graph is more appropriate. An association graph is constructed from two image graphs. Each node represents a mapping between a node in one image graph and a node in the other; i.e. a mapping between objects in one image and objects in the other. An arc between two association graph nodes represents the degree of compatibility between two mappings. The largest fully connected subgraph (maximal clique) in the association graph corresponds to the best mapping of objects in one image to those in the other. Yang, Snyder, and Bilbro (1989) have used association graphs to deal with the problem of oversegmentation. However they made "no attempt to assign merit values to the association graph nodes, or to the compatibilities between nodes. So if there are missing objects or extra regions there is no assurance that the largest clique actually represents the best match" (Ranganath & Chipman, 1992, p. 632). By assigning weights to each possible object to object mapping, i.e. each node of the association graph, a suitable updating or relaxation rule can be applied iteratively to adjust node weights until some convergence criterion is met. Davis (1979) applied discrete relaxation to an association graph in a boundary matching application. He used discrete relaxation to reduce the size of the association graph by deleting nodes and arcs – thereby decreasing the number of cliques to be evaluated. After relaxation he evaluated all cliques of the association graph using a cost formula to determine the optimal one. Price (1986) applied probabilistic relaxation to an association graph. The method requires that there be a one-to-one correspondence between the objects of the input image and those of the reference image (i.e. no segmentation errors). Initial node weights, probabilities, are assigned on the basis of this assumption. Thus in the case of extraneous objects introduced by segmentation error it becomes necessary to define *null objects*. The determination of the probability that a given object maps to a null object poses a puzzling but artificial problem. The fuzzy relaxation approach described by Ranganath and Chipman (1992) uses an updating rule that incorporates contextual information. The contextual information is provided by a set of real-valued attributes (attribute vector) for each object; e.g. length, area, circularity, texture (i.e. rotation and translation invariant measures). Each node of the association graph, i.e. object-to-object mapping, is assigned a weight based on the cumulative sum of the absolute differences between object attributes (differences are normalised to be in the interval [0,1]). Similarly each arc is assigned a normalised weight based on the cumulative sum of differences between relationships between pairs of objects. After fuzzy relaxation nodes with weights below a chosen threshold are discarded and the sum of the node weights for each fully connected subgraph (clique) of the association graph is calculated. The clique with the highest sum is then deemed to be the best mapping of objects from one image to the other – no cost formula is used. The fuzzy relaxation method is able to deal with problems of mismeasured attributes, missing objects, and false objects. Moreover by making slight, intuitively and analytically natural modifications to the method it can deal with over- and undersegmentation errors.

We are currently investigating the fuzzy relaxation method as means of matching pairs of vein signatures (medial axis representations). As an example consider the line segment representations of the two vein signatures shown in Figure 19.

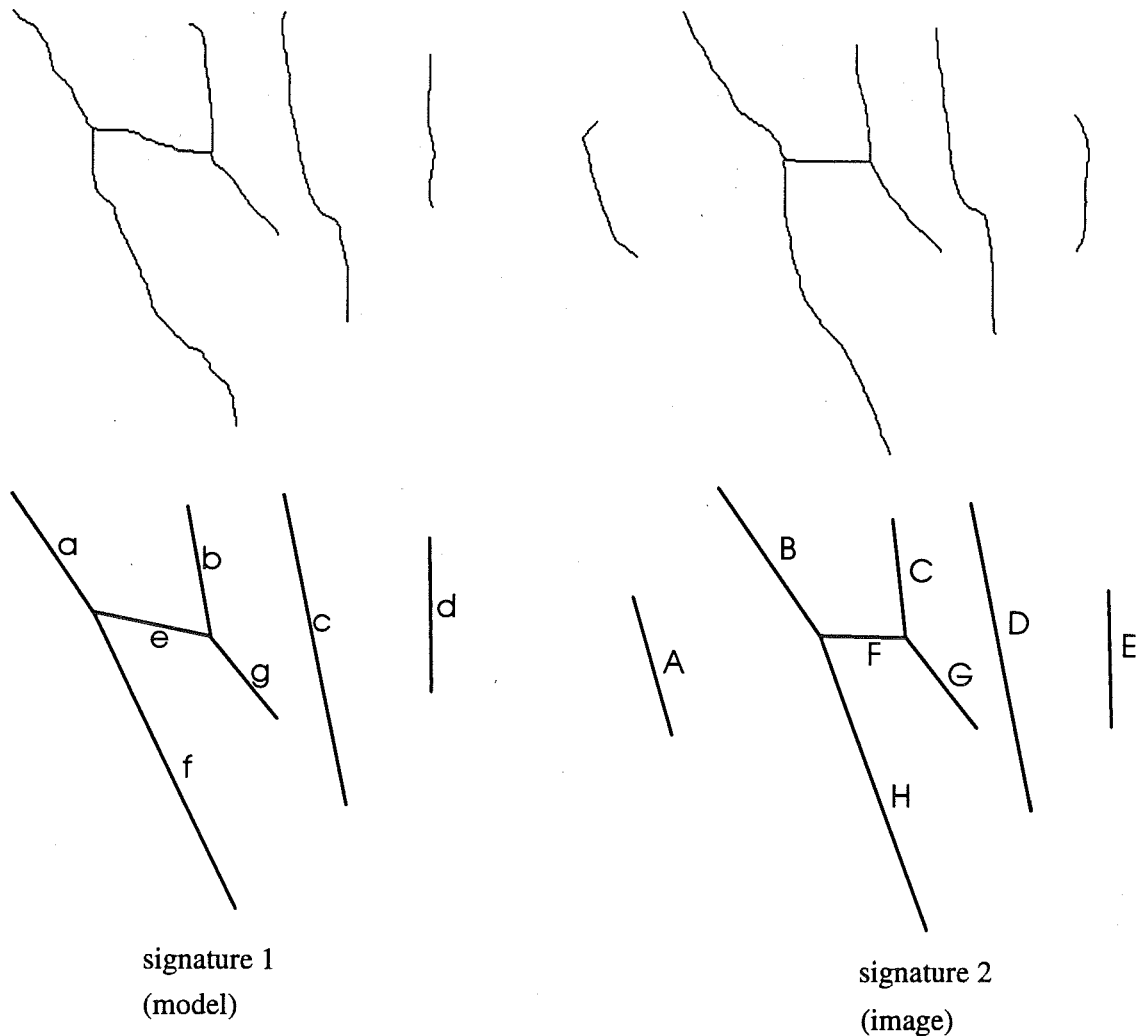


Figure 19. Two vein signatures, from the same hand, and their respective line segment representations.

To simplify the discussion let signature 1 be called the *model* and signature 2 be called the *image*. Further the labelled line segments of the model are *objects* whilst those of the image are *regions*. The association graph for the model/image pair is a *complete graph* with $7 \times 8 = 56$ nodes and $56 \times (56 - 1) \times \frac{1}{2} = 1540$ arcs. Tables 3 and 4 list the length and angle of orientation with respect to the horizontal for the objects and regions respectively. *Length* and *angle* are attributes (measured in pixel size units and degrees respectively). Tables 5 to 8 list the distance and angle relations for the objects and regions respectively. The distance relation is defined to be the length of the line segment joining the midpoints of two objects or two regions (symmetric matrix). The angle relation is defined to be the positive angle this line forms with the horizontal. Note however that the angle relation matrix is not symmetric. For example, as Figure 20 shows, the angle between A and B is not the same as that between B and A (their difference however is always 180°).

Table 3. Object attributes for signature 1 (model) of Figure 19.

	length	angle
a	91.0	123.3
b	80.2	100.0
c	199.3	101.9
d	96.0	90.6
e	76.1	170.2
f	208.0	115.9
g	67.6	128.4

Table 4. Region attributes for signature 2 (image) of Figure 19.

	length	angle
A	91.4	107.8
B	113.7	124.2
C	73.6	97.0
D	195.3	100.6
E	84.0	90.0
F	55.0	179.0
G	199.3	110.3
H	72.6	128.3

Table 5. Distance relation for the objects of signature 1 (model) depicted in Figure 19.

	a	b	c	d	e	f	g
a	0.0	93.7	177.5	242.5	76.7	149.2	143.7
b	93.7	0.0	88.9	148.9	44.9	122.1	71.7
c	177.5	88.9	0.0	76.7	105.4	118.8	48.2
d	242.5	148.9	76.7	0.0	177.1	193.1	124.9
e	76.7	44.9	105.4	177.1	0.0	87.4	67.2
f	149.2	122.1	118.8	193.1	87.4	0.0	73.9
g	143.7	71.7	48.2	124.9	67.2	73.9	0.0

Table 6. Angle relation for the objects of signature 1 (model) depicted in Figure 19.

	a	b	c	d	e	f	g
a	0.0	353.0	339.7	351.0	324.5	298.2	327.4
b	173.0	0.0	325.8	349.7	227.3	259.4	293.0
c	159.7	145.8	0.0	17.8	170.7	216.1	199.4
d	171.0	169.7	197.8	0.0	182.1	209.0	198.4
e	144.5	47.3	350.7	2.1	0.0	275.3	330.6
f	118.2	79.4	36.1	29.0	95.3	0.0	46.9
g	147.4	113.0	19.4	18.4	150.6	226.9	0.0

Table 7. Distance relation for the regions of signature 2 (image) depicted in Figure 19.

	A	B	C	D	E	F	G	H
A	0.0	100.2	166.8	222.1	292.1	135.8	159.7	184.8
B	100.2	0.0	83.3	158.8	225.4	76.1	155.4	133.6
C	166.8	83.3	0.0	80.7	143.3	42.7	130.0	70.4
D	222.1	158.8	80.7	0.0	70.0	88.4	113.8	41.0
E	292.1	225.4	143.3	70.0	0.0	158.1	170.2	108.6
F	135.8	76.1	42.7	88.4	158.1	0.0	93.3	57.8
G	159.7	155.4	130.0	113.8	170.2	93.3	0.0	77.1
H	184.8	133.6	70.4	41.0	108.6	57.8	77.1	0.0

Table 8. Angle relation for the regions of signature 2 (image) depicted in Figure 19.

	A	B	C	D	E	F	G	H
A	0.0	41.6	19.2	1.7	1.1	8.0	332.4	356.9
B	221.6	0.0	352.1	337.8	344.3	321.4	295.3	325.1
C	199.2	172.1	0.0	323.1	339.8	237.4	262.9	292.6
D	181.7	157.8	143.1	0.0	359.2	171.9	225.0	203.7
E	181.1	164.3	159.8	179.2	0.0	175.1	207.8	188.2
F	188.0	141.4	57.4	351.9	355.1	0.0	274.3	329.9
G	152.4	115.3	82.9	45.0	27.8	94.3	0.0	56.1
H	176.9	145.1	112.6	23.7	8.2	149.9	236.1	0.0

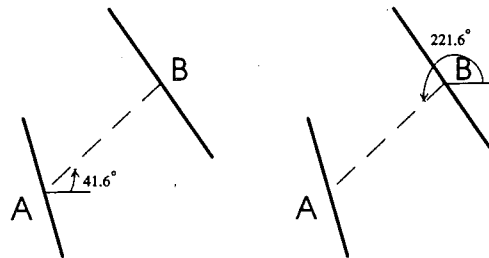


Figure 20. The angle relation for the mapping A to B and the mapping B to A respectively.

The fuzzy relaxation approach to determining the best mapping of regions to objects using the association graph is as follows:

1. Calculate the initial node weights

For each node of the association graph, i.e. a region-to-object mapping, a weight is calculated based on the cumulative sum of the absolute difference in attributes. For node pair (i, j) the initial mapping weight is given by the equation

$$S(i, j)^{(0)} = \frac{n - \sum_{k=1}^n |x_k(i) - y_k(j)| W_k}{n},$$

where x_k and y_k are the k -th attributes of the i -th region of the image (signature 2) and the j -th object of the model (signature 1) respectively, W_k is a weighting constant used for scaling and indicating the relative importance of the k -th attribute, and n is the number of attributes. For example the node (A,b) has weight:

$$S(1,2)^{(0)} = \frac{2 - (|91.4 - 80.2| + |208.0 - 55.0| + |107.8 - 100.0| + |179.0 - 90.0|)}{2} = 0.92,$$

where, in this case, the normalising factor W_k is the reciprocal difference between the observed maximum and minimum for the k -th attribute for all objects and regions.

2. Calculate arc weights or compatibility coefficients

For each arc between nodes (i, j) and (h, k) a weight is calculated based on the absolute sum of differences between relations. The value of this weight is determined by the differences in the relations between regions i and h , and objects j and k . The calculation is similar to that for node

weights but uses relation values corresponding to pairs of regions and pairs of objects rather than attribute values. For example the arc (A,b;B,c) is assigned the weight:

$$C(1,2;2,3) = \frac{2 - (|100.2 - 88.9| + (292.1 - 41.0) + |41.6 - 325.8| + (180))}{2} \approx 0.77.$$

Note: because the arctan function is not continuous the absolute difference of the angle relation must be subtracted from 360° if it is greater than 180°; e.g. |41.6 - 325.8| is interpreted as (360.0 - 284.2).

Once again the normalising factors are based on maximum and minimum values. To prevent mappings of a given region to more than 1 object the value of $C(i, j; i, k)$ is defined to be 0. Similarly $C(i, j; h, j)$ is defined to be 0.

3. Update node weights using the fuzzy relaxation rule

Node weights are updated according to the rule

$$S(i, j)^{(r+1)} = \alpha S(i, j)^{(0)} + (1 - \alpha) \left[\frac{1}{L} \sum_{h=1}^L \left(\max_{k=1}^K (S(h, k)^{(r)} C(i, j; h, k)) \right) \right],$$

where α is a constant in the interval [0,1], L is the number of regions and K is the number of objects. After all the node weights have been updated they are normalised so that their sum remains constant. This is accomplished by multiplying each node weight by the factor:

$$\frac{\sum_{i=1}^L \sum_{j=1}^K S(i, j)^{(0)}}{\sum_{i=1}^L \sum_{j=1}^K S(i, j)^{(r+1)}}.$$

4. Test the relaxation termination condition

Test the condition

$$|S(i, j)^{(r+1)} - S(i, j)^{(r)}| < \delta,$$

where δ is a predefined small number; e.g. 0.001. If the condition is not satisfied return to step 3.

5. Evaluation of the result

Using a predetermined threshold value discard all nodes that have low weights. Next find all the cliques in the remaining association graph. The clique with the highest sum of node weights is deemed to be the best mapping of regions to objects.

Appendix B contains a listing of an ANSI C program used to generate the initial and final node weights for the mapping of regions to objects for the image and model shown in Figure 19. The results for $\alpha = 0.15$ and $\delta = 0.001$ are shown in Table 9. For a threshold value of 0.85 the maximal clique is: (B,a), (C,b), (D,c), (E,d), (F,e), (G,f), (H,g). Thus region A does not map to any object – it is an extraneous region.

Table 9. Final node weights for the mapping of regions (signature 2) to objects (signature 1).

Node (object mapping)	Initial node weight	Final node weight
S(A,a)	0.91	0.79
S(A,b)	0.92	0.65
S(A,c)	0.61	0.52
S(A,d)	0.89	0.50
S(A,e)	0.60	0.65
S(A,f)	0.57	0.63
S(A,g)	0.81	0.60
S(B,a)	0.92	0.85
S(B,b)	0.75	0.74
S(B,c)	0.59	0.57
S(B,d)	0.75	0.53
S(B,e)	0.62	0.72
S(B,f)	0.65	0.62
S(B,g)	0.83	0.63
S(C,a)	0.80	0.67
S(C,b)	0.96	0.88
S(C,c)	0.56	0.68
S(C,d)	0.89	0.65
S(C,e)	0.58	0.71
S(C,f)	0.45	0.58
S(C,g)	0.80	0.72
S(D,a)	0.53	0.51
S(D,b)	0.62	0.69
S(D,c)	0.98	0.89
S(D,d)	0.62	0.69
S(D,e)	0.22	0.58
S(D,f)	0.87	0.65
S(D,g)	0.43	0.71
S(E,a)	0.79	0.48
S(E,b)	0.93	0.65
S(E,c)	0.56	0.72
S(E,d)	0.96	0.87
S(E,e)	0.52	0.52
S(E,f)	0.45	0.53
S(E,g)	0.73	0.66
S(F,a)	0.57	0.64
S(F,b)	0.47	0.72
S(F,c)	0.10	0.58
S(F,d)	0.37	0.49
S(F,e)	0.88	0.87
S(F,f)	0.15	0.59
S(F,g)	0.67	0.74
S(G,a)	0.57	0.57
S(G,b)	0.55	0.62
S(G,c)	0.95	0.74
S(G,d)	0.55	0.55
S(G,e)	0.26	0.63
S(G,f)	0.94	0.89
S(G,g)	0.47	0.70
S(H,a)	0.91	0.59
S(H,b)	0.82	0.73
S(H,c)	0.44	0.72
S(H,d)	0.71	0.61
S(H,e)	0.75	0.73
S(H,f)	0.49	0.65
S(H,g)	0.98	0.89

Notes.

- (i) Results are for $\alpha = 0.15$ and $\delta = 0.001$ (required 5 iterations for convergence).
- (ii) Shaded cells indicate final weights greater than or equal to 0.85.

6.4. Discussion

An advantage of the fuzzy relaxation method (FRM) over the sequential correlation matching method (SCMM) is that registration need not be performed. Matching is done on the basis of the attributes and distance and angle relationships within a signature and not on absolute spatial location. We believe though that registration is necessary to prevent mismatching in cases similar to that of Figure 17. If this turns out to be the case then perhaps the coordinates of the midpoints of the objects and regions (line segments) could be used as attributes. A large sample study is required to gauge the performance of this method and to compare it against the SCMM. Naturally this will entail determining and comparing the FAR and FRR for the two methods as well as making a comparison on the basis of computational speed and efficiency. In the preceding example the vein signatures were amenable to a simple line segment representation. However when dealing with a signature like that of Figure 21 the simple decomposition of the signature into line segments between junctions and endpoints is clearly not adequate. Consequently a more sophisticated encoding scheme needs to be devised. In addition further research is needed to develop strategies for determining the optimal attributes, relations, weighting factors, and value of α for the FRM.

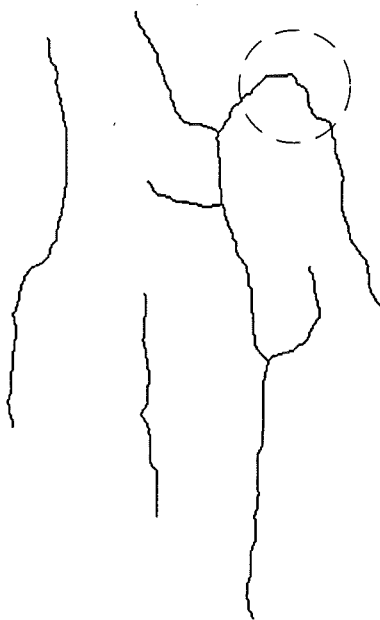


Figure 21. An example of a signature that is not amenable to line segment decomposition using endpoints and junctions.

Our present study indicates the need to improve the image acquisition system particularly with regard to registration; at least as far as the SCMM is concerned. An obvious way of improving registration is to raise the height of the existing docking frame. Alternatively the thumb and the side of the hand adjacent to the thumb could be used to locate a hand for imaging (Figure 22). The lighting system also needs to be improved. The current system, because it uses a single IR source, induces surface shadows and some specular reflection; for example the plateau evident in the centre of Figure 8(a) is due to specular reflection. This affects the performance of the segmentation algorithm leading to segmentation errors. "Even lighting calls for an adequate number of lights, an equal amount of illumination on both sides of the camera-subject axis, and a proper distribution of lighting over the subject." (Newman, 1976, p. 82). When illuminating a convex surface using infrared Newman has suggested using a lighting angle of about 55° as shown in Figure 23. To minimise specular reflection the camera should be given a little forward slant (Newman, 1976, p. 86). Infrared polarising filters need to be investigated as a means of reducing specular reflection. Another possibility for reducing intense reflection is to provide electronic attenuation of the intensity of the IR source(s). For example the frame-grabbing software could readily measure the entropy and histogram characteristics of a captured image and then use this information to adjust the

lighting level. Alternatively the lighting intensity could be encoded on a smart-card along with an individual's library template.

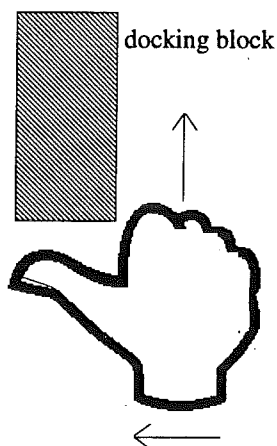


Figure 22. An alternative method of positioning the hand for imaging.

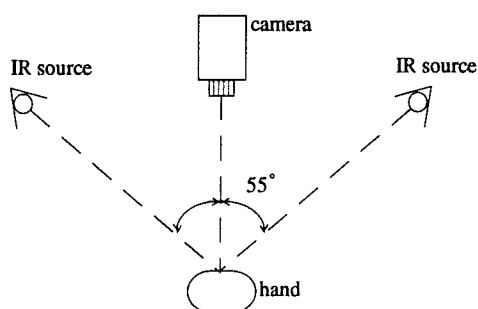


Figure 23. Ideal lighting angle for imaging the back of a hand.

7. VEXED

Whilst DIMPAL provided a useful research environment for algorithm development, it was not fast enough for our purposes (several minutes to extract a signature). DIMPAL operators and functions are designed to handle images of different sizes and data types. The cost incurred by this generality is that of additional computational overhead. To obtain speed improvements it was necessary to extract the necessary source code from DIMPAL and to modify it to work on fixed size $640H \times 480V$ byte images. The resulting program, *VEXED*, short for vein extraction and equivalence determination, is written in ANSI C for IBM's Operating System/2 (OS/2) version 2.x. This operating system was chosen because it provides a flat linear 32-bit memory address space, a 32-bit graphics engine, and pre-emptive multitasking. DOS source code provided by Data Translation for interfacing to the DT2855 frame-grabber served as a basis for the development of custom native OS/2 interface code. *VEXED* can acquire an image and extract the medial axis representation of the vein pattern in around 120 seconds (as opposed to nearly 10 minutes in DIMPAL). Tophat transformation is by far the most computationally expensive part of the segmentation algorithm. Van Herk (1992) devised a fast algorithm for local maximum and minimum filters on rectangular and octagonal kernels. The algorithm reduces the computational complexity of the closing for the tophat transformation to only 12 maximum and 12 minimum operations per pixel. Even so real-time processing ultimately requires the use of a real-time morphological

processor. Kuczborski, Attikiouzel, and Crebbin (1992) have proposed a VLSI architecture for implementing grey-scale mathematical morphology using a redundant number representation. Edith Cowan University in conjunction with the University of Adelaide are currently working on a gallium arsenide VLSI design based on this novel data representation.

8. SUMMARY AND CONCLUSION

Our prototype biometric system, *VEXED*, demonstrates that a commercial back-of-hand biometric system is technically viable. The requisite hardware is low cost and readily available off-the-shelf. *VEXED* is able to capture, store, and process infrared back-of-hand images, build and store library templates, and perform sequential correlation matching of stored or newly acquired signatures against a library of signature templates. The system exploits the near infrared sensitivity of the INTERLINE TRANSFER CCD chip for the purpose of obtaining more highly contrasted images of vein structure than could otherwise be seen with the naked eye. The custom segmentation algorithm is based on Mathematical Morphology and incorporates a novel noise removal filter⁷ built from a maximum of linear closings followed by a minimum of linear openings. Registration is performed by translating the centroid of the domain of the digital image of a hand to a common origin and rotating about this origin until the axis joining the centroid to the midpoint at the wrist is vertical. Vein patterns are stored as medial axis representations. A library template is constructed from several independently acquired signatures. Matching involves comparing a given signature against either a single template (as would be the case for a smart-card) or a library of templates (as in the case of a database). Matching is two-fold: a signature to be verified is matched against a dilated template (forward match), using constrained sequential correlation, and then the template is matched against the dilated test signature (reverse match). A successful match requires both the forward and reverse match percentages to be high. Our estimates of the FAR and FRR for *VEXED* are initial estimates only because they are based on a small sample size; namely 20 people and 100 hand images. A more detailed study is required, using images from more than 100 people, to determine the most appropriate forward and reverse match percentages and to more reliably estimate the FAR and FRR. In addition the optimal sizes of the structuring elements used in the segmentation algorithm, and in particular the size of the octagon used in the tophat transform, need to be determined.

It is important to realise that near infrared imaging doesn't guarantee that vein patterns will be boldly delineated and contrasted. Indeed in a preliminary study prior to the cross-matching experiment of section 6.2., we obtained 5×34 images of the backs of hands from 34 students in order to evaluate the effectiveness of near infrared imaging. For one of the 34 students no vein pattern could be discerned from any of the IR images. One of the conditions known to reduce or obscure the venous pattern is a relatively thick layer of subcutaneous fat (Newman, 1976, p. 118). Further research needs to be done to determine the optimal band of the actinic range for imaging subcutaneous veins. This will involve the testing of IR sources with different operating wavelengths in conjunction with an extensive range of IR filters and possibly CCD cameras. If, after refining the imaging system, there are still individuals whose vein structure cannot be seen then the usefulness of this biometric system as a method of access control will be severely diminished. Consequently it will be necessary to combine the vein signature (or the fact that there is no signature) with a secondary trait such as the outline of the hand, or its area, or the shape of the knuckles; or with a more traditional access control method such as a PIN. Alternatively the vein pattern of the palm of the hand or at the wrist could be investigated as a means of biometric identification. The existing segmentation and matching strategies would still be relevant though some parameters would need to be modified; e.g. the size of the structuring element used for tophat transformation.

Opportunities for further research include:

1. Redesigning the image acquisition unit:
 - identifying the ideal band of actinic infrared for imaging the subcutaneous veins (this will determine the choice of IR filter);
 - constructing a two-source IR lighting system as in Figure 23;
 - investigating the use of polarising filters to reduce specular reflection;
 - implementing software control of the intensity of the IR source(s);

⁷ The filter is not a morphological filter in the sense of Serra (1988) because it is not idempotent.

- implementing and testing the docking block design (Figure 22) as well as other design ideas for constraining a hand for imaging.
- 2. Improving the segmentation algorithm:
 - adding a grey-level dimension to the line segment structuring elements; e.g. saw-tooth, ramp, parabola;
 - investigating segmentation using the *watershed transform* (Meyer & Beucher, 1990; Dougherty, 1993).
- 3. Researching additional registration and matching algorithms:
 - exploring fuzzy relaxation on association graphs further;
 - exploring the possibility of using neural networks to identify signatures.
- 4. Developing a real-time back-of-hand vein pattern biometric system:
 - purchasing/developing a real-time morphological processor;
 - modifying the existing segmentation and matching algorithms to take advantage of the morphological processor.
- 5. Validation and testing:
 - using a statistically representative sample of individuals to test the integrity of the system – in particular obtain refined estimates of the FAR and FRR.

9. REFERENCES

- Davis, L.S. (1979). Shape matching using relaxation techniques. *IEEE Trans. PAMI*, 1(1), 60-72.
- Dougherty, E.R. (Ed.). (1993). *Mathematical morphology in image processing*. New York: Marcel Dekker, Inc.
- Fak, V. (1991). Computer verification of human users' identity: a theoretical model and some evaluation criteria. *Computers and Security*, 10, 626-636.
- Fukunaga, K. (1991). Image matching using structures of edge-image graphs. *Systems and Computers in Japan*, 22, 61-71.
- Gottesfeld Brown, L. (1992). A survey of image registration techniques. *ACM Computing Surveys*, 24(4), 325.
- Hawkes, P.L. & Clayden, D.O. (1993, September). *Veincheck research for automatic identification of people*. Paper presented at the Hand and Fingerprint Seminar at NPL.
- Kuczborski, W., Attikiouzel, Y., & Crebbin, G. (1992). Video rate morphological processor based on a redundant number representation. In B.G. Batchelor, M.J. Chen, & F.W. Waltz (Eds.), *Machine vision, architectures, integration, and applications* (pp. 249-260). Bellingham: SPIE.
- Lake, D. (1994). How can I see what I'm looking at? Lighting and image accuracy, quality. *Advanced Imaging*, 9(5), 34-38.
- Lau, H.T. (1989). *Algorithms on graphs*. Blue Ridge Summit, PA: TAB Professional and Reference Books.
- MacGregor, P. & Welford, R. (1991). Veincheck: Imaging for security and personnel identification. *Advanced Imaging*, 6(7), 52-56.
- MacGregor, P. & Welford, R. (1992). Veincheck lends a hand for high security. *Sensor Review*, 12(3), 19-23.
- Mehnert, A.J. (1994a). *DIMPAL: Digital image processing and analysis language* [Computer program]. Perth, WA: A.J. Mehnert, c/o Department of Mathematics, Edith Cowan University.

- Mehnert, A.J. (1994b). *Digital morphometry: a taxonomy of morphological filters and feature parameters with application to Alzheimer's disease research*. Unpublished Masters thesis, Edith Cowan University, Perth, WA.
- Mehnert, A.J., Cross, J.M., & Smith, C.L. (1993). *Thermographic imaging: segmentation of the subcutaneous vascular network of the back of the hand* (Research Report). Perth, Western Australia: Edith Cowan University, Australian Institute of Security and Applied Technology.
- Meyer, F. & Beucher, S. (1990). Morphological segmentation. *Journal of Visual Communication and Image Representation*, 1(1), 21-46.
- Miller, B. (1994). Vital signs of identity. *IEEE Spectrum*, 31(2), 22-30.
- Newman, A.A. (Ed.). (1976). *Photographic techniques in scientific research* (vol. 2). London: Academic Press
- Parks, J.R. (1991). Personal identification – biometrics. In Lindsay, D.T. and Price, W.L. (Eds.) *Information security*, pp. 181-191. North Holland: Elsevier Science Publishers.
- Pierce, C. (1993). *CCTV sales/application*. Davenport, Iowa: L.T.C. Training Centre
- Price, K.E. (1986). Hierarchical matching using relaxation. *Computer Vision, Graphics and Image Processing*, 34(1), 66-75.
- Ranganath H.S. & Chipman L.J. (1992). Fuzzy relaxation approach for inexact scene matching. *Image and Vision Computing*, 10(9), 631-640
- Serra, J. (1982). *Image analysis and mathematical morphology*. London: Academic Press.
- Serra, J. (Ed.). (1988). *Image analysis and mathematical morphology. Volume 2: Theoretical advances*. London: Academic Press.
- Simpson, L. (1994). The Fingerscan personal ID system. *Silicon Chip*, 7(5), 8-9.
- Sossa, J.H. (1989). An improved parallel algorithm for thinning digital patterns. *Pattern Recognition Letters*, 10, 77-80.
- Van Herk, M. (1992). A fast algorithm for local minimum and maximum filters on rectangular and octagonal kernels. *Pattern Recognition Letters*, 13, 517-521.
- Yang, B., Snyder, W.E., & Bilbro, G.L. (1989). Matching oversegmented 3D images to models using association graphs. *Image and Vision Computing*, 7(2), 135-143.
- Zhang, T.Y. & Suen, C.Y. (1984). A fast parallel algorithm for thinning digital patterns. *Communications of the ACM*, 27(3), 236-239.

APPENDIX A

Mathematical Morphology

"As originally conceived by Georges Matheron, mathematical morphology concerns the analysis of binary images by means of probing with structuring elements" (Dougherty, 1993, preface). The theory has since been extended to grey-tone images (functions) and most recently Serra and Matheron (Serra, 1988) have generalised the theory to complete lattices.

Consider an ink pen drawing on a piece of white paper; a binary image. The image can be modelled by a set of points in \mathbf{R}^2 , where \mathbf{R} is the set of real numbers, which locate the image foreground. Now consider a black-and-white photograph. Black-and-white is a misnomer as the photograph actually consists of grey tones. This image can be modelled by a function $f: \mathbf{R}^2 \rightarrow \mathbf{R}$. When an image is digitised, it is sampled at a finite number of points and the brightness value at each point is mapped to a discrete value. A digital binary image can be represented by a set of points in \mathbf{Z}^2 , where \mathbf{Z} is the set of integers, and a digital grey-tone image can be represented by a discrete-valued function $\hat{f}: \mathbf{Z}^2 \rightarrow \mathbf{Z}$. In the definitions that follow, $A, B \subset \mathbf{Z}^2$ represent discrete binary images (sets of foreground points), and the functions $f: \mathbf{Z}^2 \rightarrow \mathbf{Z}$ and $g: \mathbf{Z}^2 \rightarrow \mathbf{Z}$ represent discrete grey-tone images. Furthermore, A (resp. f) is called the *image* and B (resp. g) is called the *structuring element*. The operation $+$ (resp. $-$) denotes either vector addition (resp. subtraction) or arithmetic addition (resp. subtraction). The two elementary operations of mathematical morphology are the *dilation* and the *erosion*.

Definition 1. Dilation.

$$\mathcal{D}(A, B) = A \oplus B = \bigcup_{b \in B} A_b, \text{ and}$$

$$\mathcal{D}(f, g)(\mathbf{x}) = (f \oplus g)(\mathbf{x}) = \max_{\substack{\mathbf{z} \in \text{domain}(g) \\ (\mathbf{x} - \mathbf{z}) \in \text{domain}(f)}} \{f_{\mathbf{z}}(\mathbf{x}) + g(\mathbf{z})\},$$

where $\mathbf{x} = (x, y) \in \mathbf{Z}^2$, $A_b = \{\mathbf{a} + \mathbf{b} \mid \mathbf{a} \in A\}$, $f_{\mathbf{z}}(\mathbf{x}) = f(\mathbf{x} - \mathbf{z})$.

Definition 2. Erosion.

$$\mathcal{E}(A, B) = (A \ominus \bar{B}) = \bigcap_{b \in B} A_{-b} = \{\mathbf{x} \mid B_{\mathbf{x}} \subset A\}, \text{ and}$$

$$\mathcal{E}(f, g)(\mathbf{x}) = (f \ominus \bar{g})(\mathbf{x}) = \min_{\mathbf{z} \in \text{domain}(g)} \{f_{-\mathbf{z}}(\mathbf{x}) - g(\mathbf{z})\},$$

where $\bar{B} = \{-\mathbf{b} \mid \mathbf{b} \in B\}$ and $\bar{g}(\mathbf{x}) = g(-\mathbf{x})$.

The two most elementary morphological image filters are the *opening* and the *closing*. These are translation invariant, increasing (preserve order relations), and idempotent mappings.

Definition 3. Opening.

$$\mathcal{O}(A, B) = \mathcal{D}(\mathcal{E}(A, B), B),$$

$$\mathcal{O}(f, g) = \mathcal{D}(\mathcal{E}(f, g), g).$$

Definition 4. Closing.

$$\mathcal{C}(A, B) = \mathcal{E}(\mathcal{D}(A, B), B),$$

$$\mathcal{C}(f, g) = \mathcal{E}(\mathcal{D}(f, g), g).$$

When the structuring element g only takes on the value zero on its domain (i.e. it is flat) it can be expressed by a point set $B \subset \mathbf{Z}^2$ (its domain). The grey-level dilation and erosion given in definitions 1 and 2 then reduce to

$$\mathcal{D}(f, B)(\mathbf{x}) = (f \oplus B)(\mathbf{x}) = \max\{f(\mathbf{y}) \mid \mathbf{y} \in \tilde{B}_{\mathbf{x}}\}, \text{ and}$$

$$\mathcal{E}(f, B)(\mathbf{x}) = (f \ominus \tilde{B})(\mathbf{x}) = \min\{f(\mathbf{y}) \mid \mathbf{y} \in B_{\mathbf{x}}\}.$$

Morphological gradient (Beucher's gradient)

By definition the gradient of a function $f(x, y)$ is the vector $\nabla f = \left(\frac{\partial f}{\partial x}, \frac{\partial f}{\partial y}\right)$. For a given point $P(x, y)$, the norm of the vector gives the value of the maximal directional derivative of f at P :

$$|\nabla f(P)| = \sqrt{\left(\frac{\partial f}{\partial x}\bigg|_P\right)^2 + \left(\frac{\partial f}{\partial y}\bigg|_P\right)^2}.$$

Beucher (1978) proposed the following algorithm for calculating the norm of ∇f (cited in Serra, 1982, p. 441):

$$|\nabla f| = \lim_{\lambda \rightarrow 0^+} \frac{\mathcal{D}(f, \lambda B) - \mathcal{E}(f, \lambda B)}{2\lambda},$$

where B is the unit disk. The digital version of Beucher's gradient (Serra, 1988, p. 312) is given by:

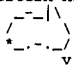
$$\frac{\mathcal{D}(f, B) - \mathcal{E}(f, B)}{2}$$

where B is a 3×3 cross-shaped (or square) structuring element.

APPENDIX B

Implementation of the fuzzy relaxation method in C

```

/* =====
                AISAT                Edith Cowan University
                Australian Institute of Security and Applied Technology
                Perth Western Australia
                
PROJECT: Back-of-hand subcutaneous vein pattern biometric system
AUTHOR: Andrew Mehnert
SYNOPSIS: This program is an implementation of the fuzzy relaxation method applied
to association graphs described in "Fuzzy relaxation approach for inexact
scene matching", Image and Vision Computing, 10(9), 631-640.
===== */

#include <stdio.h>
#include <math.h>

#define ABS(A) (((A)<0)?-(A)):((A))
#define MAX(A,B) ((A)<(B)?(B):(A))
#define MIN(A,B) ((A)<(B)?(A):(B))

#define NUMBER_OF_ATTRIBUTES 2
#define NUMBER_OF_RELATIONS 2
#define NUMBER_OF_OBJECTS 7
#define NUMBER_OF_REGIONS 8

#define ALPHA 0.15
#define DELTA 0.001
#define PI 3.141592654

/* ...MAXIMUM MINUS MINIMUM FOR EACH ATTRIBUTE -- USED TO NORMALISE NODE WEIGHTS... */
double reciprocal_attrib_wt_constants[NUMBER_OF_ATTRIBUTES] = {208.0-55.0,179.0-90.0};

/* ...ARRAY TO HOLD NORMALISING CONSTANTS FOR RELATIONS -- CONSTANTS GENERATED BY PROGRAM... */
double reciprocal_relat_wt_constants[NUMBER_OF_RELATIONS];

/* ...3 ARRAYS: [2] HOLDS THE INITIAL NODE WEIGHTS, [0] AND [1] ARE USED TO HOLD r AND (r+1) WEIGHTS... */
double node_weights[3][NUMBER_OF_REGIONS][NUMBER_OF_OBJECTS];

double arc_weights[NUMBER_OF_REGIONS][NUMBER_OF_OBJECTS][NUMBER_OF_REGIONS][NUMBER_OF_OBJECTS];

/* ...FIRST TWO ATTRIBUTES ARE USED TO COMPUTE NODE WEIGHTS; THE MIDPOINT COORDINATES ARE USED
TO GENERATE OBJECT DISTANCE AND ANGLE RELATIONS. THE INITIALISATION DATA IS FOR SIGNATURE 1
OF FIGURE 19... */
double object_attributes[NUMBER_OF_ATTRIBUTES+2][NUMBER_OF_OBJECTS] =
(
    /* LENGTH */
    {91.0, 80.2, 199.3, 96.0, 76.1, 208.0, 67.6},
    /* ANGLE */
    {123.3, 100.0, 101.9, 90.6, 170.2, 115.9, 128.4},
    /* x COORDINATE OF MIDPOINT */
    {278, 371, 444.5, 517.5, 340.5, 348.5, 399},
    /* y COORDINATE OF MIDPOINT */
    {-137,-148.5,-198.5,-175,-181.5,-268.5,-214.5}
);

double object_relations[NUMBER_OF_RELATIONS][NUMBER_OF_OBJECTS][NUMBER_OF_OBJECTS];

/* ...FIRST TWO ATTRIBUTES ARE USED TO COMPUTE NODE WEIGHTS; THE MIDPOINT COORDINATES ARE USED
TO GENERATE REGION DISTANCE AND ANGLE RELATIONS. THE INITIALISATION DATA IS FOR SIGNATURE 2
OF FIGURE 19... */
double region_attributes[NUMBER_OF_ATTRIBUTES+2][NUMBER_OF_REGIONS] =
(
    /* LENGTH */
    {91.4, 113.7, 73.6, 195.3, 84.0, 55.0, 199.3, 72.6},
    /* ANGLE */
    {107.8, 124.2, 97.0, 100.6, 90.0, 179.0, 110.3, 128.3},
    /* x COORDINATE OF MIDPOINT */
    {220, 295, 377.5, 442, 512, 354.5, 361.5, 404.5},
    /* y COORDINATE OF MIDPOINT */
    {-221.5, -155, -166.5, -215, -216, -202.5, -295.5, -231.5}
);

double region_relations[NUMBER_OF_RELATIONS][NUMBER_OF_REGIONS][NUMBER_OF_REGIONS];

/* =====
PROGRAM STARTS HERE:

(1) Calculate initial node weights and store in node_weights[0] and node_weights[2]
(2) Calculate angle and distance relations for objects and regions independently
(3) Calculate arc weights between all nodes of the association graph
(4) Iteratively update node weights until the difference between the r and (r+1)
weights is less than DELTA
===== */

void main(void)
{
int    i,j, h, k, l,          /* ..USED TO INDEX ARRAYS.. */
    new_node_weights,        /* ..TOGGLES BETWEEN 1 AND 0 TO INDICATE LATEST WEIGHTS, I.E.
                                node_weights[0] or node_weights[1].. */
    converged,                /* ..1 = CONVERGED.. */

```

```

iteration;          /* ..ITERATION COUNTER.. */

double absolute_sum_of_differences,
difference,
max_difference,
sum_of_initial_node_weights,
sum_of_new_node_weights,
x_diff,
y_diff,
x_squared,
y_squared,
sum,
product,
max_product,
normalising_factor,
distance,
max_dist,
min_dist,
theta;

/* ..CALCULATE INITIAL MAPPING WEIGHTS S(i,j) (I.E. NODE WEIGHTS).. */
sum_of_initial_node_weights = 0.0;
for(i=0; i < NUMBER_OF_REGIONS; i++)
  for (j=0; j < NUMBER_OF_OBJECTS; j++)
  {
    absolute_sum_of_differences = 0.0;
    for (k=0; k < NUMBER_OF_ATTRIBUTES; k++)
      absolute_sum_of_differences += ABS(region_attributes[k][i] - object_attributes[k][j]) /
        reciprocal_attrib_wt_constants[k];

    node_weights[0][i][j] = node_weights[2][i][j] =
      (NUMBER_OF_ATTRIBUTES - absolute_sum_of_differences) /
        NUMBER_OF_ATTRIBUTES;
    sum_of_initial_node_weights += node_weights[0][i][j];
  }

/* ..CALCULATE DISTANCE RELATION (MIDPOINT-TO-MIDPOINT) AND ANGLE RELATION FOR REGIONS AND
THEN FOR OBJECTS.. */

max_dist=0.0;
min_dist=800.0; /*.. SIGNATURE IMAGE BUFFER IS 640X x 480V --> LENGTH OF DIAGONAL IS sqrt(640^2+480^2).. */

for(i=0; i < NUMBER_OF_REGIONS; i++)
  for (j=0; j < NUMBER_OF_REGIONS; j++)
    if (i != j)
    {
      x_diff = region_attributes[2][j] - region_attributes[2][i];
      x_squared = x_diff*x_diff;

      y_diff = region_attributes[3][j] - region_attributes[3][i];
      y_squared = y_diff*y_diff;

      distance = sqrt(x_squared + y_squared);
      max_dist = MAX(max_dist,distance);
      min_dist = MIN(min_dist,distance);
      theta = atan2(y_diff,x_diff)*180/PI;
      if (theta < 0)
        theta += 360;
      region_relations[0][i][j] = distance;
      region_relations[1][i][j] = theta;
    }

printf("REGION RELATIONS\n-----\n");
printf("Distance relation\n");
for(i=0; i < NUMBER_OF_REGIONS; i++)
  {
    for (j=0; j < NUMBER_OF_REGIONS; j++)
      printf("%5.1f,", region_relations[0][i][j]);
    printf("\n");
  }

printf("\nAngle relation\n");
for(i=0; i < NUMBER_OF_REGIONS; i++)
  {
    for (j=0; j < NUMBER_OF_REGIONS; j++)
      printf("%5.1f,", region_relations[1][i][j]);
    printf("\n");
  }

for(i=0; i < NUMBER_OF_OBJECTS; i++)
  for (j=0; j < NUMBER_OF_OBJECTS; j++)
    if (i != j)
    {
      x_diff = object_attributes[2][j] - object_attributes[2][i];
      x_squared = x_diff*x_diff;

      y_diff = object_attributes[3][j] - object_attributes[3][i];
      y_squared = y_diff*y_diff;

      distance = sqrt(x_squared + y_squared);
      max_dist = MAX(max_dist,distance);
      min_dist = MIN(min_dist,distance);
      theta = atan2(y_diff,x_diff)*180/PI;
      if (theta < 0)
        theta += 360;
      object_relations[0][i][j] = distance;
      object_relations[1][i][j] = theta;
    }

printf("\nOBJECT RELATIONS\n-----\n");
printf("Distance relation\n");
for(i=0; i < NUMBER_OF_OBJECTS; i++)
  {
    for (j=0; j < NUMBER_OF_OBJECTS; j++)
      printf("%5.1f,", object_relations[0][i][j]);
    printf("\n");
  }

printf("\nAngle relation\n");
for(i=0; i < NUMBER_OF_OBJECTS; i++)
  {

```

```

    for (j=0; j < NUMBER_OF_OBJECTS; j++)
        printf("%5.1f,", object_relations[1][i][j]);
    printf("\n");
}

/* ..NOW CALCULATE NORMALISING CONSTANTS FOR EACH RELATION.. */
reciprocal_relat_wt_constants[0] = (max_dist - min_dist);

max_difference = 0.0;
for (i=0; i < NUMBER_OF_REGIONS; i++)
    for (j=0; j < NUMBER_OF_OBJECTS; j++)
        for (h=0; h < NUMBER_OF_REGIONS; h++)
            for (k=0; k < NUMBER_OF_OBJECTS; k++)
                {
                    difference = ABS(region_relations[1][i][h] - object_relations[1][j][k]);
                    if (difference > 180.0)
                        difference = 360.0 - difference;
                    max_difference = MAX(max_difference, difference);
                }
reciprocal_relat_wt_constants[1] = max_difference;
printf("Relation normalising factors: Distance --> %6.4f; Angle --> %6.4f\n",
    reciprocal_relat_wt_constants[0], reciprocal_relat_wt_constants[1]);

/* ..CALCULATE ARC WEIGHTS FOR THE ASSOCIATION GRAPH.. */

printf("\nARC WEIGHTS\n-----\n");

for (i=0; i < NUMBER_OF_REGIONS; i++)
    for (j=0; j < NUMBER_OF_OBJECTS; j++)
        for (h=0; h < NUMBER_OF_REGIONS; h++)
            for (k=0; k < NUMBER_OF_OBJECTS; k++)
                {
                    if (i==h || j==k)
                        arc_weights[i][j][h][k]=0.0;
                    else
                        {
                            absolute_sum_of_differences = 0.0;
                            for (l=0; l < NUMBER_OF_RELATIONS; l++)
                                {
                                    difference =
                                        ABS(region_relations[1][i][h] - object_relations[1][j][k]);
                                    if (l == 1 && difference > 180.0)
                                        difference = 360.0 - difference;
                                    absolute_sum_of_differences += difference/
                                        reciprocal_relat_wt_constants[1];
                                }
                            arc_weights[i][j][h][k] = (NUMBER_OF_RELATIONS -
                                absolute_sum_of_differences)/
                                NUMBER_OF_RELATIONS;
                        }
                    printf("C(%c,%c,%c,%c) = %6.4f\n", 'A'+i, 'a'+j, 'A'+h, 'a'+k,
                        arc_weights[i][j][h][k]);
                }

/* ..APPLY FUZZY RELAXATION TO THE ASSOCIATION GRAPH.. */

new_node_weights = 1;
iteration = 0;
converged = 0;

while (!converged)
    {
        sum_of_new_node_weights = 0.0;

        for(i=0; i < NUMBER_OF_REGIONS; i++)
            for (j=0; j < NUMBER_OF_OBJECTS; j++)
                {
                    sum = 0.0;
                    for (h=0; h < NUMBER_OF_REGIONS; h++)
                        {
                            max_product = 0.0;
                            for (k=0; k < NUMBER_OF_OBJECTS; k++)
                                {
                                    product = node_weights[!new_node_weights][h][k] *
                                        arc_weights[i][j][h][k];
                                    max_product = MAX( max_product, product);
                                }
                            sum += max_product;
                        }

                    node_weights[!new_node_weights][i][j] = ALPHA*node_weights[2][i][j] +
                        (1-ALPHA)*sum/NUMBER_OF_REGIONS;
                    sum_of_new_node_weights += node_weights[!new_node_weights][i][j];
                }

        /* NORMALISE NEW NODE WEIGHTS AND TEST FOR CONVERGENCE */

        converged = 1;
        normalising_factor = sum_of_initial_node_weights / sum_of_new_node_weights;
        for(i=0; i < NUMBER_OF_REGIONS; i++)
            for (j=0; j < NUMBER_OF_OBJECTS; j++)
                {
                    node_weights[!new_node_weights][i][j] *= normalising_factor;
                    if (ABS(node_weights[!new_node_weights][i][j] -
                        node_weights[!new_node_weights][i][j]) >= DELTA)
                        converged = 0;
                }

        new_node_weights = !new_node_weights;
        iteration++;

        printf("Iteration %d\n-----\n", iteration);

        for(i=0; i < NUMBER_OF_REGIONS; i++)
            for (j=0; j < NUMBER_OF_OBJECTS; j++)
                printf("S(%c,%c) %4.2f --> %4.2f\n", 'A'+i, 'a'+j, node_weights[2][i][j],
                    node_weights[!new_node_weights][i][j]);
    }
}

```